PINK1 Phosphorylates MIC60/Mitofilin to Control Structural Plasticity of Mitochondrial Crista Junctions

Pei-I Tsai[1], Chin-Hsien Lin[2], Amanda M. Papakyrikos[1,3], Carmen Schoor[4], Julien Couthouis[5], Ruey-Meei Wu[2], Zbigniew K. Wszolek[6], Dominic Winter[4], Owen A. Ross[7], and Xinnan Wang[1]*

1. Department of Neurosurgery, Stanford University School of Medicine, Palo Alto, U.S.A.;
2. Department of Neurology, National Taiwan University Hospital, Taipei, Taiwan;
3. Graduate Program in Developmental Biology, Stanford University School of Medicine, Palo Alto, U.S.A.;
4. Institute for Biochemistry and Molecular Biology, University of Bonn, Bonn, Germany;
5. Department of Genetics, Stanford University School of Medicine, Palo Alto, U.S.A;
6. Department of Neurology, Mayo Clinic, Jacksonville, FL 32224, USA;
7. Department of Neuroscience, Mayo Clinic, Jacksonville, FL 32224, USA.

* Correspondence: xinnanw@stanford.edu

ABSTRACT

Mitochondrial crista structure partitions vital cellular reactions and is precisely regulated by diverse cellular signals. Here we show that in *Drosophila*, the Parkinson's disease (PD)-linked Ser/Thr kinase PINK1 phosphorylates the inner mitochondrial membrane protein MIC60/mitofilin to maintain crista junctions by stabilizing MIC60 oligomerization. This role of PINK1-mediated phosphorylation is most critical in high-energy regions of the cell that contain

mitochondria with condensed cristae and large numbers of crista junctions. Expression of MIC60 restores crista structure and ATP levels of *PINK1* null flies, and remarkably rescues their behavioral defects and dopaminergic neurodegeneration. Furthermore, in an extension to human disease, we discover that *MIC60* mutations in the mitochondrial targeting sequence may increase the risk of PD in humans, and expression of disease-linked human *MIC60* mutations in *Drosophila* impairs crista junction formation and causes locomotion deficits. These findings highlight the importance of maintenance and plasticity of crista junctions to cellular homeostasis *in vivo*.

INTRODUCTION

Efficient mitochondrial oxidative phosphorylation and ATP synthesis rely heavily on the exquisite membrane organization of mitochondrial cristae. Inner mitochondrial membrane (IMM) protrudes into the matrix to form cristae that harbor the electron transport chain (ETC) machinery and ATP synthase. Each individual crista contains a tubular invagination, with an opening to the intermembrane space called crista junction and a bottom called crista tip (Fig. 1a). Crista membranes bend extensively at crista junctions and tips to sustain the remarkably narrow and elongated crista space, and this unique shape is required for maintenance of solute gradients and localization of the ETC complexes [1]. Studies in yeast have revealed several crucial factors involved in maintenance of crista structure, including the mitochondrial contact site and cristae organizing system (MICOS) complex, mitochondrial fission-fusion machinery, F_oF_1-ATP synthase, and mdm33 [2-12]. Mitochondrial crista structure is not always static, instead, it undergoes dynamic remodeling tightly correlated with the mitochondrial aerobic respiration rates [12-17]. In high-energy cells, mitochondria perform higher respiratory activities. However, it

remains elusive how cellular signals instruct mitochondria to remodel crista architecture, particularly in an *in vivo* setting.

Mutations in the Ser/Thr kinase PINK1 cause autosomal recessive early-onset PD [18]. The hallmark of PD is age-dependent degeneration of dopaminergic (DA) neurons in the substantia nigra. PINK1 is imported into healthy mitochondria with the polarized mitochondrial membrane potential ($\Delta\Psi m$) [19-23]; and it is blocked from import into damaged mitochondria with the depolarized $\Delta\Psi m$ and stabilized on the outer mitochondrial membrane (OMM) [24-35]. One well-known role of PINK1 is to trigger mitophagy that clears depolarized mitochondria by phosphorylating its substrates on the mitochondrial surface [24-35]. However, whether PINK1 has kinase activity inside healthy mitochondria remains controversial. Although PINK1 has been shown to be crucial for the mitochondrial complex I activity [22, 36-40], direct PINK1 kinase substrates in the ETC have not yet been identified [22, 36, 39]. In this work, we discover a novel substrate of PINK1 inside healthy mitochondria—the IMM protein MIC60/mitofilin, and we reveal that the PINK1-MIC60 pathway maintains remodeling of crista junctions, the complex I activity, and dopaminergic neuronal survival *in vivo*.

RESULTS

PINK1 Localizes to the OMM, Intermembrane Space, and Matrix in *Drosophila*.

First, we determined whether PINK1 is present inside mitochondria in *Drosophila*. By immuno-gold staining under Transmission Electron Microscopy (TEM), we found that transgenic PINK1-Flag was evenly distributed inside the mitochondria, likely in the matrix or intermembrane space, as well as outside the mitochondria in the cytosol (Supplementary Fig. 1a). Human PINK1

transgene was used here and throughout the paper owing to the functional conservation between human and fly PINK1 [41]. Using proteinase K and membrane extraction assays [22], we found that endogenous *Drosophila* PINK1 (dPINK1) was present on the OMM, in the intermembrane space, and in the matrix; however, it was not integrated into the membrane (Supplementary Fig. 1b-c).

Inside Healthy Mitochondria PINK1 Is Required for Maintenance of Crista Junctions in High-Energy Areas.

We next examined mitochondrial crista structure under TEM, and identified novel crista phenotypes in body wall muscles of *PINK1* null late third instar larvae 120 hrs after egg laying (AEL). Approximately 34.45% of total mitochondria appeared like an "onion" with concentric multi-layered and heavily-packed crista membranes, and 58.13% were filled with small "vacuole"-like crista membranes. In both cases, crista junctions were significantly reduced. In *PINK1* null mitochondria there were only 1.03±0.29 crista junctions/μm of mitochondrial circumference, while in wild-type mitochondria there were 5.08±0.32 crista junctions/μm (Fig. 1b-d, Supplementary Fig. 2a). These results indicate that PINK1 is required for maintenance of crista junctions in late third instar larval body wall muscles. The mitochondrial shape became round in *PINK1* null larvae, although the mitochondrial size was not significantly altered compared with that of wild-type (Supplementary Fig. 2b). No pronounced muscle degeneration was observed in *PINK1* null larvae (Supplementary Fig. 2c). We found the same "onion"- and "vacuole"-like mitochondria in larval body wall muscles using another independent *PINK1* null allele (Supplementary Fig. 3). In the nervous system, the phenotype of the "onion"-like cristae and loss of crista junctions existed only in the neuropils (enriched with synapses, dendrites, and axons) at the ventral nerve cords (VNC), but not in the cell bodies at the VNC, in the segmental

nerves (axons), or at the neuromuscular junctions (NMJs) in *PINK1* null larvae (Supplementary Fig. 4). We then considered the possibility that mitochondrial cristae undergo PINK1-dependent remodeling when mitochondria move from the cell bodies into the neuropils. To explore this possibility, we measured the mitochondrial crista density (the number of cristae/mitochondrial area) and found that mitochondria in neuropils contained significantly more dense cristae with increased crista junctions than those in neuronal cell bodies, axons, or NMJs (Supplementary Fig. 5a), indicating that mitochondrial remodeling of crista structure occurs when mitochondria move into neuropils and mitochondrial respiratory activity increases [13-17]. In addition, neuropils had more mitochondria (the volume mitochondria occupy/total volume) than neuronal cell bodies, axons, or NMJs (Supplementary Fig. 5b), suggesting that synapse and dendrite-enriched neuropils consume more energy [42, 43]. Therefore, when mitochondria move to subcellular compartments that may have elevated energy demands, they condense their cristae and increase crista junctions in third instar larvae. This structural plasticity requires PINK1, because in those regions of *PINK1* null larvae mitochondrial cristae fail to remodel as in wild-type, and instead they display the "onion"-like membranes with loss of crista junctions (Fig. 1, Supplementary Fig. 2-4). Taken together, PINK1 is essential for maintaining crista junctions in high-energy subcellular domains in third instar larvae (Fig. 1e).

We next determined the extent to which the physical presence of PINK1 inside the healthy mitochondria is required for maintenance of crista junctions. To do this, we ubiquitously expressed full-length PINK1, or PINK1$^{\Delta MTS}$ without the mitochondrial targeting sequence (MTS) that leads PINK1 import into mitochondria [20, 44], in *PINK1* null larvae. Both *PINK1* transgenes were inserted in the same genomic site using the PhiC31 integrase-mediated transgenesis systems to ensure the same genomic regulations [45], and their protein expression levels were

comparable (Supplementary Fig. 6a). The aberrant crista structure and loss of crista junctions in *PINK1* null flies were fully rescued by expressing full-length PINK1, but not PINK1$^{\Delta MTS}$ in late third instar larval body wall muscles (Fig. 1b-d, Supplementary Fig. 2a). Therefore, the import of PINK1 into healthy mitochondria is required for maintenance of crista junctions in muscles.

The "onion" and "vacuole"-like mitochondria with significant loss of crista junctions found in *PINK1* null larvae differed from the previously reported "vacuolated (empty)" mitochondria with crista fragmentation phenotype in thoracic indirect flight muscles of *PINK1* null adults [41, 46] (Supplementary Fig. 6b, c). Notably, in "vacuolated" mitochondria, although crista membranes were broken into small pieces, many crista junctions were kept intact (Supplementary Fig. 6b) [41]. The reason that *PINK1* null adults show different crista phenotypes in muscles from *PINK1* null larvae could be because the larval muscles are not similar as those in adults. Most larval body wall muscles are destructed once pupariation starts and new muscles are formed for adults. Furthermore, mitochondria in thoracic indirect flight muscles face tremendous stress because of the intense activities of these muscles in adults. Nevertheless, the predominant presence of the "vacuolated" mitochondria in *PINK1* null adult muscles suggests that PINK1 has additional functions at the adult stage, and thus we focused our study on the larval stage when PINK1 plays a primary role in maintaining crista junctions (Fig. 1b-d).

It has been reported that *Parkin* null adult flies exhibit similar "vacuolated" mitochondria with crista fragmentation as *PINK1* null adults [41, 46-48]. To answer the question of whether *Parkin* null larvae also show the "onion" and "vacuole"-like mitochondria in their muscles as observed in *PINK1* null larvae, we performed TEM on *Parkin* null third instar larval body wall muscles. Surprisingly, about half of total mitochondria were normal (40.07%), and majority of abnormal mitochondria (38.44%) displayed a "dumbbell" shape in which two ends of one mitochondrion

stretch extensively in the opposite directions while the OMM and crista junctions are intact (Fig. 1f), implying a failure in fission. Thus, *PINK1* and *Parkin* mutant larvae show distinct phenotypes in crista structure.

To determine whether this role of PINK1 in flies has been conserved in humans, we performed TEM on induced pluripotent stem cell (iPSC)-derived human *PINK1* null neurons and their isogenic wild-type controls. Because these cultured neurons intermix and form extensive networks in the dish, it is difficult to reliably discern the precise subcellular regions under TEM. Even so, we detected 19.00% of total neuronal mitochondria exhibiting the "onion"-like structure with loss of crista junctions in *PINK1* null neurons, while only 1.73% of total mitochondria in wild-type displayed this morphology (Supplementary Fig. 7). Notably, RNAi knockdown of *PINK1* in non-neuronal HeLa cells has been reported to cause crista fragmentation without dramatically affecting crista junction formation [49]. Therefore, the role of PINK1 in the regulation of crista junctions in selective subcellular regions/cell types including neurons is conserved in humans. Collectively, our results show a novel function for PINK1 inside healthy mitochondria in regulating structural plasticity of mitochondrial crista junctions.

PINK1 Phosphorylates MIC60.

We next sought the mechanism by which PINK1 maintains crista junctions. Because our studies suggested a Parkin-independent mechanism, we searched additional proteins that could functionally interact with PINK1. A previous study has reported human MIC60, an IMM integral protein (also called IMMT/Fcj1/mitofilin) in the MICOS complex, in a mass spectrometry screen searching for PINK1's binding partners using cultured HEK293T cells [44]. Interestingly, the MICOS complex has been demonstrated to play a crucial role in crista junction formation [2, 4-7, 16,

[50-53]. In flies, we found that endogenous dPINK1 physically interacted with endogenous *Drosophila* MIC60 (dMIC60) *in vivo* (Fig. 2a). We achieved this result by generating a polyclonal antibody against dMIC60 protein (anti-dMIC60). A band of the predicted size of dMIC60 protein was recognized by anti-dMIC60 in wild-type but not in a *dMIC60* mutant (*dMIC60^{mut}*, described later), confirming the specificity of this antibody (Fig. 2a). We determined that dPINK1 and dMIC60 also interacted *in vitro*, and mapped the region of dMIC60 required for binding to dPINK1 (Fig. 2b). We bacterially expressed and purified N-terminal glutathione *S*-transferase (GST)-tagged dMIC60 with different truncations: GST-dMIC60$^{92\text{-}739}$ (lacking the N-terminal MTS and transmembrane–TM–domains), GST-dMIC60$^{92\text{-}223_547\text{-}739}$ (lacking the N-terminal MTS and TM, and the coiled-coil domains), or GST-dMIC60$^{92\text{-}546}$ (lacking the N-terminal MTS and TM, and the C-terminal domains) [54], and incubated it with glutathione sepharose beads before incubation with bacterially purified C-terminal V5-tagged dPINK1. We found that dPINK1 co-precipitated with GST-dMIC60$^{92\text{-}739}$ and GST-dMIC60$^{92\text{-}223_547\text{-}739}$, but not GST-dMIC60$^{92\text{-}546}$ (Fig. 2b), suggesting that the C-terminal AAs 547-739 of dMIC60 are required for directly binding to dPINK1.

Since PINK1 is a Ser/Thr kinase, we next determined whether dMIC60 is a substrate of PINK1. To do this, we performed an *in vitro* PINK1 kinase assay on bacterially expressed dMIC60. dMIC60$^{92\text{-}739}$ was incubated with purified *Tribolium castaneum* PINK1 (TcPINK1)–the known form of PINK1 that remains active *in vitro* [55], or inactive kinase-dead TcPINK1 (TcPINK1KD), prior to mass spectrometric and phos-tag acrylamide analysis. Using mass spectrometry, we identified two dMIC60 sites, Threonine 507 and 561, which were phosphorylated; these two sites were not phosphorylated in the other negative controls although the unphosphorylated peptides were detected with the same efficiency among all reactions (Fig.

2c, d, Supplementary Fig. 8). In the mass spectrometric analysis, we encompassed approximately 90% of the total residues of dMIC60$^{92\text{-}739}$. Using phos-tag acrylamide where phosphorylated proteins migrate slower because of binding to the phos-tag ligands, we detected phosphorylated dMIC60, only in the reaction with ATP and TcPINK1 both present, but not when ATP or TcPINK1 was absent (Fig. 2d). When the two phosphorylation sites were mutated to phosphorylation-resistant (PR) Alanine, dMIC60 was no longer phosphorylated by TcPINK1 (Fig. 2d), indicating that these two sites are the main phosphorylation sites.

We also compared the *in vitro* phosphorylation efficiency of dMIC60 with that of a known PINK1 substrate, ubiquitin. We found that under the same conditions dMIC60 was more efficiently phosphorylated by PINK1 than ubiquitin (Fig. 2e).

We generated two antibodies against phosphorylated dMIC60 at Threonine 507 and 561, respectively, and found that the band intensities recognized by anti-phospho-dMIC60 were completely abolished by kinase-dead TcPINK1KD *in vitro* (Fig. 2f, left), confirming the specificity of these antibodies. Phosphorylation at both sites was significantly reduced in *PINK1* null flies (Fig. 2f, right), suggesting that PINK1 is a major kinase phosphorylating these sites *in vivo*. We verified that PINK1-mediated phosphorylation of dMIC60 requires the physical presence of PINK1 inside the mitochondria, because expression of PINK1$^{\Delta MTS}$ in *PINK1* null flies failed to phosphorylate dMIC60 as detected by anti-phospho-dMIC60 (Fig. 2g). Taken together, PINK1 phosphorylates dMIC60 both *in vivo* and *in vitro*.

PINK1-Mediated Phosphorylation of MIC60 Maintains Crista Junctions.

Our finding that the IMM protein dMIC60 is a substrate of PINK1 (Fig. 2) suggests the intriguing possibility that PINK1 might maintain crista junctions by phosphorylating dMIC60. If

this hypothesis were true, blocking phosphorylation of dMIC60 by mutating the phosphorylation sites (Fig. 2) might cause similar crista phenotypes as removing PINK1. To test this hypothesis directly, we ubiquitously expressed wild-type dMIC60 ($dMIC60^{WT}$), or $dMIC60^{PR}$ (Fig. 2), in a *dMIC60* mutant background ($dMIC60^{mut}$) [56] without expression of endogenous *dMIC60* (Fig. 2a, Supplementary Fig. 9a). This allele of *dMIC60* caused loss of crista junctions ubiquitously in late third instar larvae (Fig. 3, Supplementary Fig. 9b). Both the wild-type and mutant *dMIC60* transgenes were inserted in the same genomic location [45] to ensure the same genomic regulations and their expression levels in $dMIC60^{mut}$ were comparable (Supplementary Fig. 9c). Ubiquitous expression of either transgene in $dMIC60^{mut}$ flies did not exceed the endogenous dMIC60 level (Supplementary Fig. 9c), and thus circumvented the potential adverse effect by overexpression. $dMIC60^{WT}$ in $dMIC60^{mut}$ flies completely restored their crista structure (Fig. 3, Supplementary Fig. 9b). In contrast, $dMIC60^{PR}$ in $dMIC60^{mut}$ failed to restore crista junctions only in muscles and neuropils, but could rescue crista phenotypes in neuronal cell bodies, axons, and NMJs in third instar larvae (Fig. 3, Supplementary Fig. 9b). Thus, $dMIC60^{PR}$ in $dMIC60^{mut}$ mirrors the crista phenotypes of *PINK1* null flies: mitochondria lose crista junctions in muscles and neuropils (Fig. 1, 3, Supplementary Fig. 2, 4, 9). These results provide evidence that PINK1-mediated phosphorylation of dMIC60 is required for maintenance of crista junctions in high-energy areas in *Drosophila*.

We further tested whether the role of PINK1-mediated phosphorylation of MIC60 is conserved in human cells. We knocked down endogenous human MIC60 by RNAi in HEK293T cells, and expressed RNAi-resistant either wild-type or phospho-resistant human MIC60 with the two conserved sites (Serine 518 and Threonine 587) mutated to Alanine. We found that MIC60 RNAi knockdown in HEK293T cells resulted in the “onion”-like mitochondria phenotype, which

was rescued by the expression of wild-type MIC60, but not that of phospho-resistant MIC60 (Supplementary Fig. 10a-c). Therefore, it is likely that PINK1 also maintains crista junctions via phosphorylating MIC60 in human cells.

MIC60 Rescues the Defect in Crista Structure of *PINK1* Null Flies.

Since dMIC60 is a substrate of PINK1 for maintaining crista junctions (Fig. 2-3), this places *dMIC60* genetically downstream of *PINK1*. To confirm their epistatic relationship, we ubiquitously expressed *dMIC60* in a *PINK1* null background, or *PINK1* in *dMIC60*^{mut}. Remarkably, upregulating dMIC60 completely rescued all the abnormal crista phenotypes in *PINK1* null larval and adult muscles (Fig. 4a, Supplementary Fig. 10d); on the contrary, PINK1 expression did not rescue the crista phenotypes in *dMIC60*^{mut} larval muscles (Fig. 4b). Importantly, these results suggest that overexpression of dMIC60 that is not phosphorylated by PINK1 compensates for the lack of PINK1-mediated phosphorylation. Upregulation of dMIC60 in *Parkin* null flies did not rescue their crista phenotypes in either larvae or adults (Fig. 4c, Supplementary Fig. 10e), suggesting that the restoration of crista structure in *PINK1* null flies by dMIC60 is owing to epistasis between them rather than a general improvement of mitochondrial function, and excluding the possibility that *dMIC60* acts downstream of *Parkin*. Thus, *dMIC60* functions downstream of *PINK1* to maintain crista structure in muscles.

A few other factors have also been reported as being downstream of PINK1 at the adult stage, such as Parkin [41, 46, 49, 57], the complex I [22, 36-38], the mitochondrial fission-fusion machinery [57-60], and MUL1 [61]. To determine whether these known PINK1-dependent pathways interplay with the PINK1-MIC60 pathway for crista structure maintenance in larval muscles, we expressed *Parkin* (a ubiquitin E3 ligase), *ND42* (a complex I subunit), *Sicily* (co-chaperone of ND42), *Drp1*

(controls mitochondrial fission), or *MUL1* (a ubiquitin E3 ligase) in *PINK1* null larvae. All five transgenes have been shown to rescue the mitochondrial morphological phenotypes in *PINK1* null adult muscles to varying degrees [36, 41, 46, 57, 58, 61]. In striking contrast to *dMIC60*, none of them rescued the "onion"- or "vacuole"-like mitochondria in *PINK1* null larval muscles (Fig. 4a). These results indicate dMIC60 as the strongest downstream factor of PINK1 in larvae to maintain crista structure. Consistent with the argument against Parkin as a robust genetic interactor of the PINK1-dMIC60 axis, we have observed that *dMIC60* fails to rescue the crista abnormality of *Parkin* null mutant larvae (Fig. 4c) that show distinct crista phenotypes from *PINK1* or *dMIC60* null larvae (Fig. 1, 3), and additionally we found that removing one copy of *Parkin* gene from *PINK1* null mutant larvae did not alter their phenotypes with lost crista junctions (Supplementary Fig. 10f). Now we have not only revealed the differing crista phenotypes between the muscles at the larval and adult stages of *PINK1* null flies (Fig. 1, Supplementary Fig. 6), but we have also demonstrated that their underlying causes may not be the same. At the larval stage, maintenance of crista junctions regulated by PINK1 and dMIC60 is key to crista structure; whereas at the adult stage, multiple PINK1-mediated pathways may be involved (Fig. 4d).

Both Phosphorylation and Upregulation of MIC60 Promote MIC60 Oligomerization.

Here we have shown that both PINK1-mediated phosphorylation of dMIC60 (Fig. 1-3) and overexpression of dMIC60 that is not phosphorylated by PINK1 (Fig. 4a) maintain crista junctions in high-energy cellular regions. These results suggest that upregulated and phosphorylated dMIC60 cause the same functional impact on crista junctions. Because homo-oligomerization of MIC60 has been shown to be crucial for the formation of crista junctions [4, 16,

[62], we then reasoned that upregulated and phosphorylated dMIC60 both promote dMIC60 oligomerization. We immunoblotted dMIC60 using blue-native (BN) SDS-PAGE to detect dMIC60 oligomerization. Phosphorylation of dMIC60 by wild-type TcPINK1 *in vitro* caused retardation of dMIC60 migration above 720 KDa, indicative of dMIC60 oligomers, and this oligomerization was abolished by kinase-dead TcPINK1KD (Fig. 5a). This reveals that PINK1-mediated phosphorylation of dMIC60 promotes dMIC60 oligomerization *in vitro*. To detect the dMIC60 complex *in vivo*, we immunoblotted dMIC60 from fly lysates. We found that in wild-type background dMIC60 migrated as an oligomer [62] (Fig. 5b). dMIC60 oligomerization was significantly inhibited in *PINK1* null (Fig. 5b), indicating that PINK1-mediated phosphorylation of dMIC60 promotes dMIC60 oligomerization *in vivo*. Overexpressed dMIC60 in *PINK1* null fully restored its oligomerization (Fig. 5b), mimicking the effect of phosphorylated dMIC60 on the dMIC60 complex. Importantly, overexpression of dMIC60 in *PINK1* null did not cause more phosphorylation at either Threonine 507 or 561 than that in *PINK1* null alone without dMIC60 overexpression (Fig. 5b), excluding the possibility that the restoration of oligomerization is caused by increased phosphorylation by a kinase other than PINK1. Therefore, both upregulation and phosphorylation of dMIC60 stabilize dMIC60 oligomerization (Fig. 5c), yielding the same favorable functional consequence for crista junctions.

MIC60 Rescues the Defect in the Complex I Activity of *PINK1* Null Flies.

It is known that the mitochondrial complex I activity is compromised in *PINK1* mutant flies [22, 36-38, 40]. This phenotype might be caused by the severely disorganized crista structure in *PINK1* null mutants (Fig. 1, Supplementary Fig. 2-4, 6) [41, 46, 63], at least in part, since mitochondrial crista membranes house the complex I [1, 64]. To explore this possibility, we expressed dMIC60 in

PINK1 null flies to restore their crista structure (Fig. 4a, Supplementary Fig. 10d), and found that it completely rescued the defect in the complex I activity (Fig. 5d). Intriguingly, it has been shown that overexpression of the complex I subunit ND42 in *PINK1* null flies fully rescues their complex I deficit [36]; however, ND42 overexpression fails to restore the crista structure in *PINK1* null larvae (shown by us; Fig. 4a) or adults [36]. These results indicate that in *PINK1* null flies, the crista destruction is not secondary to, but instead upstream of the complex I defect.

MIC60 Rescues ATP Deficiency, Behavioral Disability, and DA Neuronal Loss of *PINK1* Null Flies.

It is known that ATP levels and ΔΨm are significantly disrupted in *PINK1* null flies or cells (Fig. 6a, b) [22, 37, 38, 41, 46, 65, 66]. We next ubiquitously expressed dMIC60 in *PINK1* null flies and found that it fully rescued their defects in the ATP level and ΔΨm detected by tetramethylrhodamine (TMRM) (Fig. 6a, b). Loss of PINK1 also causes locomotor deficits and DA neurodegeneration in flies [41, 46, 63, 67]. Does an impaired mitochondrial crista structure underlie these phenotypes? To answer this question, we again ubiquitously expressed dMIC60 in *PINK1* null flies to restore the crista structure and determined if this could alleviate the behavioral and neurodegenerative phenotypes associated with the *PINK1* null background. We found that loss of PINK1 at the larval stage impairs the crawling ability [67] (Fig. 6c). Expression of dMIC60 completely rescued the crawling defect of *PINK1* null third instar larvae; on the contrary, expression of Parkin, ND42, or Drp1, which fails to restore the crista structure in *PINK1* null larvae (Fig. 4a), did not fully rescue their crawling deficit (Fig. 6c). These results suggest that mitochondrial crista structure is highly relevant to cellular physiology on an organismal level in larvae. Consistently in adults, upregulating dMIC60 completely restored the climbing, jumping, and flying abilities of

PINK1 null flies 5 days after eclosion, and the DA neuronal number in the protocerebral posterior lateral 1 (PPL1) cluster of *PINK1* null adult brains 15 days after eclosion (Fig. 6d-h). Importantly, expression of the non-mitochondrial-targeting mutant PINK1$^{\Delta MTS\ 44}$, which does not restore the crista structure in *PINK1* null flies (Fig. 1, Supplementary Fig. 6), did not rescue their impairments in the ΔΨm, ATP level, behavior, and DA neuronal number (Fig. 6). In summary, *dMIC60* functions downstream of *PINK1* to maintain ATP production and locomotion, and to prevent DA neurodegeneration. In a broader sense, this discovery adds a new player, MIC60, to a cellular pathway with a key role in PD.

MIC60 Variants in the MTS Increase the Risk of PD.

Our discovery of a new PINK1-MIC60 pathway crucial for mitochondrial function and neuronal integrity, suggests the possibility for a role of this pathway in PD. Recessive loss-of-function *PINK1* mutations are a well-established cause of familial forms of early-onset PD [18]. Given that dMIC60 functions downstream of PINK1, we investigated whether *MIC60* mutations are also linked to PD in humans. We first sequenced the entire coding region of the *MIC60* gene (Supplementary Table 1) in 100 familial PD probands, 250 apparently sporadic early-onset PD patients, and 350 age/gender/ethnicity-matched controls, recruited from the movement disorder clinic of the National Taiwan University Hospital. All subjects were unrelated and there was no evidence of consanguinity. All patients received standard neurological examinations including the Unified Parkinson's Disease Rating Scale (UPDRS) and the Mini-Mental Status Evaluation (MMSE). We sequenced the previously known PD-linked genes including *SNCA*, *LRRK2*, *Parkin*, *PINK1*, *DJ-1*, *ATP13A2*, *PLA2G6*, *FBXO7*, and *DNAJC6* in all patients and did not observe any mutations. However, we identified one heterozygous missense mutation in *MIC60*,

345 *c.G50T*, causing Cysteine17 to Phenylalanine substitution (p.C17F), in 1 familial PD patient with
346 an autosomal dominant pattern of inheritance (Supplementary Fig. 11a, b). To assess the genetic
347 evidence for pathogenicity of p.C17F, we genotyped this variant in additional 602 independent
348 sporadic late-onset PD patients and 581 age/gender/ethnicity-matched control subjects of
349 Taiwanese origin. We observed the heterozygous *c.G50T* mutation in 1 additional unrelated
350 sporadic late-onset PD patient. Both patients harboring the *c.G50T* mutation are male and
351 presented with typical parkinsonian features including a good levodopa response. The sporadic
352 late-onset PD patient developed dementia with cortical brain atrophy 7 years after symptom
353 onset (Supplementary Fig. 11c, d). In summary, we found the *c.G50T* (p.C17F) mutation in 1
354 familial and 1 sporadic patient out of total 952 Taiwanese PD patients (Fig.7a, Supplementary
355 Table 2). We did not observe this mutation during the screening of 931 matched control subjects.
356 The p.C17F variant is in the MTS region of MIC60. Interestingly, recent studies have
357 suggested that rare MTS variants in *CHCHD2*, the latest nominated gene, play a role in the risk
358 of PD [68]. To explore the possibility that rare MTS variants in *MIC60* also play a role in the
359 pathogenesis of PD, we sequenced the MTS in additional 859 PD patients and 871 control
360 individuals recruited at the Mayo Clinic, the United States. We identified two heterozygous MTS
361 missense mutations (p.A4V and p.R25H) in 2 sporadic PD patients and one heterozygous MTS
362 missense mutation (p.R31C) in 2 control individuals (Fig. 7a, Supplementary Table 2).
363 To further explore the role of *MIC60* MTS variants in PD, we analyzed the newly released
364 exome sequencing data from the Parkinson's Progression Markers Initiative (PPMI) study by the
365 Michael J. Fox Foundation (http://www.ppmi-info.org) [69]. This study includes 380 recently
366 diagnosed PD patients and 197 healthy controls, recruited from twenty-one clinical study sites in
367 the United States and Europe. We compared the results from the PD patients with those from the

healthy controls recruited from the same study and the publically available single nucleotide polymorphism (SNP) databases (http://evs.gs.washington.edu/EVS/; http://www.1000genomes.org). We filtered the *MIC60* variants that are novel (absent in the SNP databases) or rare (Minor Allele Frequency <0.5% reported in http://evs.gs.washington.edu/EVS/), and non-synonymous (Supplementary Table 2). We again identified one heterozygous MTS mutation (p.T11A) in 1 sporadic PD patient (Fig. 7a), which was not present in any SNP database (Supplementary Table 2).

Our analysis suggests that rare MTS variants in *MIC60* (Supplementary Table 2) may play a role in the individual susceptibility to PD. However, it is genetically challenging to definitively confer pathogenicity to a specific rare variant for an age-dependent complex disorder such as PD [70, 71]. The essential segregation analysis of rare variants in multi-family pedigrees is not possible in those cohorts of unrelated individuals with apparently distinct genetic and environmental backgrounds. Additionally, the allelic heterogeneity of PD requires extremely large cohorts to allow meaningful statistical comparisons [70]. As an alternative strategy [70], we conducted an unbiased screen in flies to determine the functional pathogenicity of those *MIC60* MTS mutations. Because all the identified variants are heterozygous, we ubiquitously expressed the human *MIC60* transgenes carrying the mutations in *Drosophila* with a heterozygous *dMIC60* mutant background (*dMIC60*^{mut}/+). All the wild-type and mutant human *MIC60* transgenes were inserted in the same genomic location [45] and expressed at relatively similar levels (Supplementary Fig. 11e). Strikingly, expression of MIC60A4V, T11A, or C17F found in PD patients in "*dMIC60*^{mut}/+" flies, but not expression of wild-type MIC60 or R31C found in healthy control subjects, led to severe adult lethality and significantly impaired the larval crawling ability, though flies with the "*dMIC60*^{mut}/+" background genotype were normal (Fig. 7b,

c). Expression of the R25H variant, found in one PD patient, compromised the larval crawling ability but not viability (Fig. 7b, c). Importantly, expression of MIC60A4V, T11A, or C17F in "*dMIC60*^{mut}/+" significantly impaired mitochondrial crista junction formation causing the "onion"-like mitochondria in late third instar larval body wall muscles, compared to wild-type MIC60 and "*dMIC60*^{mut}/+" (Fig. 7d, Supplementary Fig.11f). This mitochondrial phenotype resembles the "onion"-like mitochondria found in *PINK1* null (Fig. 1), *dMIC60*^{mut} (Fig. 3), and "*dMIC60*^{mut}*_dMIC60*^{PR}" flies (Fig. 3). Taken together, human *MIC60* MTS variants (A4V, T11A, or C17F) found in patients impair crista junction formation, locomotion, and viability in a dominant way in *Drosophila*, supporting the hypothesis that these variants are pathogenic. Our *in vivo* functional readouts thus provide a powerful strategy to confer pathogenicity of specific rare variants that are otherwise difficult to validate genetically.

We next explored the underlying pathological mechanisms by which *MIC60* MTS variants cause phenotypes in flies. Because these mutations reside in the MTS, we reasoned that they may disrupt the mitochondrial targeting ability of MIC60. To test this hypothesis, we again expressed the Myc-tagged human MIC60 transgenes harboring the MTS variants in "*dMIC60*^{mut}/+" larvae, and detected endogenous fly dMIC60 and exogenously expressed human MIC60-Myc by immunostaining in muscles. We labeled mitochondria with anti-ATP5β [22, 38], a subunit of the mitochondrial ATP synthase. We verified the specificity of the immunostaining signals of both anti-dMIC60 and anti-Myc: the anti-dMIC60 signals disappeared in *dMIC60*^{mut} flies (Supplementary Fig. 11g), and the anti-Myc signals were undetectable in non-transgenic flies (Fig. 7e). We observed that wild-type human MIC60 or MIC60R31C found in healthy controls largely localized to mitochondria, whereas MIC60A4V, T11A, C17F, or R25H found in patients exhibited a non-mitochondrial diffuse pattern (Fig. 7e), suggesting that patients-linked variants

disrupt the mitochondrial localization of MIC60. Interestingly, endogenous dMIC60 significantly localized to mitochondria in "*dMIC60*^{mut}/+" flies or when exogenous wild-type human MIC60 or MIC60R31C was present, but this mitochondrial localization was greatly reduced when human MIC60A4V, T11A, C17F, or R25H was expressed (Fig. 7e). These results demonstrate that *MIC60* MTS variants found in PD patients damage the mitochondrial targeting ability of MIC60 in a dominant negative way in *Drosophila*. Notably, the R25H variant, which causes milder organismal phenotypes (Fig. 7b-d), affected the mitochondrial localization of dMIC60 to a lesser degree than the A4V, T11A, C17F variants (Fig. 7e), suggesting that the extent of mislocalization of MIC60 correlates with the severity of cellular consequences. Our novel strategies combining human genetics and functional screen focused on a defined coding region thus identify 3 *MIC60* variants that are highly damaging *in vivo* and may increase the risk of PD in humans.

DISCUSSION

In the present study, we have determined that PINK1 phosphorylates MIC60 to maintain crista junctions in high-energy regions in *Drosophila* larvae. This mechanism represents a novel form of PINK1-mediated phosphorylation, as PINK1 is well known to mediate mitophagy by phosphorylating its substrates on the surface of unhealthy mitochondria, dependent on the $\Delta\Psi m$. In this new mechanism, PINK1-mediated phosphorylation of MIC60 is dependent on the physical presence of PINK1 inside healthy mitochondria and is likely activated by elevation of cellular energy demands (Fig. 7f).

PINK1's kinase activity is essential for the initiation of mitophagy when PINK1 is accumulated on the surface of damaged mitochondria [24, 31-35, 72]. Here we have revealed that PINK1's kinase activity is also required for a different function: to maintain crista junctions inside healthy mitochondria. We thus have expanded the growing list of reported PINK1 substrates [24, 31-35, 73]. There is a striking similarity between the flanking sequences of the two Threonine sites in dMIC60 phosphorylated by PINK1 (Fig. 2): K/R(-3)L/A(-2)A(-1)Y(+5)K(+6)L(+9). One sequence also shares some similarity with the phospho-peptide of Miro phosphorylated by PINK1 which we discovered previously (Fig. 2) [24]: K(-3)E(+1)Y(+5). It has been hypothesized that the basic Arginine 407 of human PINK1 resides in the P+1 binding motif and may be responsible for recognizing the P+1 glutamate (E) in Miro [74]. Identification of the P+1 glutamate residue in dMIC60 implies that an acidic residue at the P+1 position may be common to several PINK1's substrates.

We have shown here that overexpressed *dMIC60* is able to compensate for the loss of phosphorylation by PINK1 in *Drosophila* (Fig. 4-6). This bears a resemblance to the regulation of Parkin or ND42, which has been reported to be phosphorylated by PINK1 directly or indirectly [22, 31-33, 35]. Overexpression of wild-type Parkin or ND42 rescues some of the *PINK1* null's phenotypes [36, 41, 46], although how this is achieved by unphosphorylated Parkin or ND42 remains unclear. Here we have skimmed the surface of the mechanism by which MIC60 upregulation compensates for the lack of PINK1 phosphorylation. We have revealed that overexpressed dMIC60 mimics phosphorylated dMIC60 to stabilize MIC60 oligomerization (Fig. 5), which is essential for crista junction formation [4, 16, 62]. When phosphorylation of MIC60 is absent in *PINK1* null, overexpressed MIC60 can stabilize its own oligomerization (Fig. 5). When

MIC60 is neither phosphorylated by PINK1 nor overexpressed (*PINK1* null alone), MIC60 fails to oligomerize and crista junctions are lost (Fig. 1 and 5). Future structural work could help define the impact of PINK1-mediated phosphorylation on the stoichiometry of the MIC60 complex.

A recent study has shown that PKA phosphorylates MIC60 to inhibit PINK1 stabilization on damaged mitochondria in cultured HeLa cells [75], placing PKA and MIC60 upstream of PINK1. In contrast, other studies have shown that activation of PKA rescues mitochondrial pathology in SH-SY5Y cells or primary neurons deficient in *PINK1* [76, 77], suggesting that PKA functions downstream of PINK1. In this work, we have revealed that MIC60 is downstream of PINK1 inside healthy mitochondria to maintain crista junctions and neuronal integrity in *Drosophila*. These varying results may reflect distinct roles PINK1 plays under different cellular environments and stresses.

We have revealed that PINK1-mediated phosphorylation of MIC60 is most critical in high energy-demanding areas such as neuropils or muscle cells (Fig. 3, 7f). In contrast, in low energy-demanding regions PINK1-mediated phosphorylation is dispensable (Fig. 3, 7f). This novel form of regulation by PINK1 phosphorylation implies that PINK1 is active inside healthy mitochondria in some cells/subdomains, but inactive in others. Selective activation of PINK1 in a subpopulation of mitochondrial pool has also been demonstrated by the findings showing that PINK1 is activated on the surface of only depolarized, but not polarized mitochondria to trigger mitophagy. The temporal and spatial regulation of PINK1 phosphorylation of its various

substrates in order to meet unique cellular needs may explain why PINK1 protein has been spotted at multiple subcellular locations [20-23, 26, 76-78] (this study).

In high-energy areas, PINK1-mediated phosphorylation of MIC60 may be required to stabilize the larger number of crista junctions, and its impairment destabilizes all crista junctions, resulting in the "onion"-like mitochondria. It is also possible that PINK1-mediated phosphorylation of MIC60 promotes formation of new crista junctions. Because the efficient condensation of cristae in mitochondria with acute respirations requires expansions in both crista junctions and membranes, when the PINK1-MIC60 pathway is impaired, synthesis of extra crista membranes may outpace formation of new crista junctions, leading to collapse of the crista membrane curvatures and consequently the "onion"-like mitochondria. Aging DA neurons in the substantia nigra demand exceedingly high rates of mitochondrial respiration, at the expense of maintaining their intense neuronal activities and elaborate axonal networks [79-81], and thus may be extremely susceptible to failure to remodel crista structure.

Intriguingly, we have discovered the same "onion"-like mitochondria in flies expressing human *MIC60* damaging variants, as in flies defective in PINK1-mediated phosphorylation of MIC60. We have further provided the pathological mechanisms by which these variants disrupt crista structure. They impair the mitochondrial targeting ability of MIC60 in a dominant negative way, consequently blocking MIC60 from entering mitochondria and from acting in concert with PINK1 (Fig. 7). Our study sheds light on a novel PD-relevant pathology that lies in mitochondrial crista structure and on perhaps one of the regulatory signals of crista structure that relies on cellular energy demands. Plasticity of crista structure must be seamlessly tailored to

shifts in energy needs in high-energy neurons, to allow for vigorous alterations in their activities and circuitry. Our work thus implicates the vital importance of mitochondrial crista structure and its ability to remodel for dynamically balancing the metabolic homeostasis of a cell.

ACKNOWLEDGEMENTS

We thank Drs. Bingwei Lu, Jongkyeong Chung, Ming Guo, Sang Ki Park, Hugo Bellen, Leo Pallanck, and Tom Clandinin for reagents, and John Perrino and the Stanford Cell Science Imaging EM Facility (1S10RR026780-01, the National Center for Research Resources) for assistance with the EM work. This work was supported by National Institute of Health (R00 NS067066) (X.W.), the Department of Defense (PR150380) (X.W.), the William N. and Bernice E. Bumpus Foundation (X.W.), the Alfred P. Sloan Foundation (X.W.), the Shurl and Kay Curci Foundation (X.W.), the Klingenstein Foundation (X.W.), the Marie Curie Career Integration Grant (D.W.), the Junior Group leader Fellowship of the Bonfor-Program at the University Hospital Bonn (D.W.), and the Postdoctoral Research Abroad Program of the National Science Council, Taiwan (P.T.). The Mayo Clinic Florida is Morris K. Udall Parkinson's Disease Research Center of Excellence (NINDS P50 #NS072187) (Z.K.W, O.A.R.), supported by the NIH/NINDS R01 NS078086 (O.A.R.) and Mayo Clinic Neuroscience Focused Research Team (Z.K.W, O.A.R.). Some data used in the preparation of this article were obtained from the PPMI database (www.ppmi-info.org/data). For up-to-date information on the study, visit www.ppmi-info.org. PPMI – a public-private partnership – is funded by the Michael J. Fox Foundation for Parkinson’s Research and funding partners, including Abbvie, Avid, Biogen, Bristol-Myers Squibb, COVANCE, GE Healthcare, Genentech, GlaxoSmithKline, Lilly, Lundbeck, Merck, Meso Scale Discovery, Pfizer, Piramal, Roche, Servier, and UCB.

AUTHOR CONTRIBUTIONS

P.T. designed and performed the experiments, made the figures and wrote the manuscript. C.L. and R.W. sequenced genes from the Taiwanese patients. A.P. performed part of the fly experiments. C.S. and D.W. performed mass spectrometry. J.C analyzed the PPMI data. Z.W. and O.R. sequenced the Mayo Clinic cohort. O.R. analyzed the overall human genetics data. X.W. conceived and supervised the project, designed the experiments, and wrote the paper with the assistance from all authors.

NO COMPETING FIANCIAL INTERESTS

EXPERIMENTAL PROCEDURES

Generation of dMIC60 Antibodies

Polyclonal dMIC60 antibody was generated by 21st Century Biochemicals (Marlborough, MA) against three peptides of dMIC60 (CAAKPKDNPLPRDVVEL, TASVSDKYWRNVEKARNY, and CLRLKRAIDSVRGDNDS). Phospho-dMIC60 antibodies were generated by Thermo Fisher Scientific (Rockford, IL) against phospho-dMIC60Thr507 (LEDKLA[pT]EKANYK) or phospho-dMIC60Thr561 (ASVRAA[pT]PGVHYK). Antibodies were immuno-depleted against non-phosphorylated peptides.

Fly Stocks

The following fly stocks were used: *Tubulin-GAL4, Actin-GAL4, elav-GAL4, da-GAL4, UAS-mitoGFP, UAS-mCD8RFP* (Bloomington Drosophila Stock Center, BDSC), *dMIC60*^{LL02849}

(Drosophila Genomics Resource Center, DGRC, Kyoto) [56], *PINK1*^{PE704} [41], *PINK1*^{5} [41], *PINK1*^{RV} [46], *PINK1*^{B9} [46], *Park*^{25}, *Park*^{rva} [47]. *UAS-hPINK1*^{WT}*-Flag, UAS-hPINK1*$^{\Delta MTS}$*-Flag, UAS-dMIC60*^{WT}*-Myc*, *UAS-dMIC60*^{T507A,T561A}*-Myc*, *UAS-hMIC60*^{WT}*-Myc*, *UAS-hMIC60*^{A44V}*-Myc UAS-hMIC60*^{T11A}*-Myc*, *UAS-hMIC60*^{C17F}*-Myc*, *UAS-hMIC60*^{R25H}*-Myc, UAS-hMIC60*^{R31C}*-Myc* were generated using PhiC31 integrase-mediated transgenesis, with an insertion at an estimated position of 25C6 at the attP40 site (BestGene, Inc.) [45].

Constructs

pUASTattB-dMIC60-Myc was generated by cloning *Drosophila* MIC60 cDNA from pOT-dMIC60 (Flybase ID: GH04666) using polymerase chain reaction (PCR), engineered with a C-terminal Myc tag and EcoRI/XbaI restriction sites at either side (New England BioLabs), into a pUASTattB vector [82]. pUASTattB-MIC60-Myc was generated by cloning human MIC60 from pcDNA3.1-MIC60-Myc [83] using PCR, engineered with BglII/XbaI restriction sites at either side, into a pUASTattB vector. pUASTattB-hPINK1-Flag or pUASTattB-hPINK1$^{\Delta MTS}$-Flag was generated by cloning either the full length human PINK1 cDNA or a fragment encoding AAs 112-581, and the C-terminal Flag, from the hPINK1-Flag construct [44], engineered with KpnI/XbaI restriction sites at either side, into a pUASTattB vector. Mutant cDNA was generated using site-directed mutagenesis with primers carrying the specific mutations (Supplementary Table 1). GST-dMIC60 truncated constructs were generated by ligating the PCR-amplified dMIC60 fragments with EcoRI/NotI restriction sites at either side into pGEX6P-1 (GE Healthcare). dMIC60-His-V5 was generated by cloning dMIC60 cDNA into pET101-TOPO (Invitrogen). dPINK1-His-V5 was generated by cloning dPINK1 cDNA, PCR amplified from wild-type (*w*^{1118}) flies, into pET101-TOPO (Invitrogen).

574

575 **Analysis of the ΔΨm Using TMRM**

576 Modified from [84]. Briefly, third instar wandering larvae were dissected in Schneider's medium
577 (Sigma) with 5 mM EGTA at 22°C in a chamber on a glass slide, then washed and incubated for
578 20 min with fresh Schneider's medium containing 5 mM EGTA, 20 nM TMRM (Molecular
579 Probes). Next, the solution was replaced with 5 nM TMRM in Schneider's medium for live
580 imaging. For TMRM quantification, the fluorescence intensity of an individual mitochondrion
581 was normalized to that of the adjacent cytoplasmic region.

582

583 **Detection of the ATP Level**

584 ATP level was measured using a luciferase-based bioluminescence assay (ATP Determination
585 Kit, Life Technologies) as previously described [67]. For each experiment, five 5-day-old adult
586 flies were homogenized in 100 µl lysis buffer (6 M guanidine-HCl, 100 M Tris pH 8.0, and
587 4 mM EDTA). The extracts were boiled for 5 min, placed on ice for 5 min, and centrifuged at
588 20,000 g for 15 min. The supernatant was then diluted to 1:500 in reaction buffer (provided by
589 the kit) and luciferase was added for 1 min. Luminescence was immediately measured using a
590 Glomax Multi Jr. Reader (Promega). Each reading was normalized to protein concentration
591 measured by bicinchoninic acid (BCA) assay (Thermo Scientific).

592

593 **Immunocytochemistry and Confocal Microscopy**

594 Adult brains or larval muscles were dissected in PBT (0.3% Tween 20 in PBS), and incubated
595 with fixative solution (4% formaldehyde in PBT) for 20 min, followed by 1 hr blocking with 1%
596 BSA in PBT. Samples were immunostained with rabbit anti-TH (AB152; EMD Millipore

Corporation) at 1:200, mouse anti-ATP5β (ab14730; AbCam) at 1:100, rabbit anti-dMIC60 at 1:500, rat anti-Myc (ab10910; AbCam) at 1:100, and Alexa 488/Cy3/Alexa 647-conjugated anti-rat (ab150165; AbCam)/mouse/rabbit IgG (Fisher) at 1:500. Samples were imaged with a 20×/N.A.0.60 or a 63×/N.A.1.30 oil Plan-Apochromat objective on a Leica SPE laser scanning confocal microscope (JH Technologies) with identical imaging parameters among different genotypes in a blind fashion. Images were processed with Photoshop CS4 using only linear adjustment of contrast.

Mitochondrial Isolation, Proteinase K Accessibility Assay, Membrane Extraction, and In-Gel Activity Assay.

Mitochondria were purified from one hundred 5-day-old adult flies or pupae homogenized in mitochondrial isolation buffer (MIB; 70 mM sucrose, 210 mM Mannitol, 50 mM Tris/HCl pH 7.5, 10 mM EDTA/Tris pH 7.5) with a glass dounce homogenizer, followed by first centrifugation at 600 g for 10 min to remove debris and another centrifugation at 7,000 g for 10 min to pellet mitochondria. Supernatant was saved as "cytosolic fraction". For Proteinase K (PK) accessibility assay, isolated mitochondria were treated with 100 μg/ml Proteinase K in MIB at 4°C for 30 min. A hypotonic rupture of the OMM was achieved by resuspensing mitochondria in 2 mM HEPES/KOH pH 7.4. Triton X-100 at a final concentration of 0.3% (v/v) was used to disrupt the IMM. PK was inactivated by incubating the reaction with 1 mM Pefabloc at 4°C for 5 min. Samples were prepared for SDS-PAGE analysis by precipitation with 10% trichloroacetic acid, followed by cold acetone washes, and resuspension in SDS sample buffer (300 mM Tris/HCl pH 6.8, 25% glycerol, 10% SDS, 0.1% bromophenol blue, and 14.4 mM 2-mercaptoethanol). For sodium carbonate (Na_2CO_3) extraction, isolated mitochondria were treated

620 with 100 mM Na_2CO_3 pH 11.5 for 30 min on ice, and then centrifuged at 17,000 g for 60 min.
621 Supernatant is enriched with soluble proteins in the intermembrane space and matrix, and pellet
622 is enriched with integral and associated proteins of the OMM and IMM. Samples were run in
623 SDS-PAGE. For dMIC60 oligomerization detection, adult flies were lysed in BN-PAGE sample
624 buffer (Thermo Fisher Scientific) with 1% Digitonin. Samples were run in 3-12% BN-Bis-Tris-
625 PAGE (Thermo Fisher Scientific). For in-gel activity, mitochondrial pellets were resuspended in
626 200 μl lysis buffer (50 mM NaCl, 50 mM imidazole/HCl pH 7.0, 2 mM 6-aminocaproic acid,
627 and 1 mM EDTA), incubated for 15 min on ice, and solubilized by adding 50 μl 10%
628 dodecylmaltoside (DDM). Mitochondrial fractions were cleared by centrifugation at 16,000 g at
629 4°C for 30 min, and mixed with 20 μl loading dye (50% glycerol and 0.1 % Ponceau S). 50 μg of
630 mitochondrial proteins from each genotype was resolved in a 4%–13% native gel using a cathode
631 buffer (50 mM Tricine, 7.5 mM imidazole, pH 7.0) containing 0.05% (w/v) deoxycholate and
632 0.01% DDM. Complex I in-gel activity assay was performed by incubating gel strips in complex
633 I reaction buffer (2.5 mg/ml nitrotetrazolium blue, 0.1 mg/ml NADH, and 5 mM Tris/HCl pH 7.4)
634 for 5 min, followed by fixation in 50% methanol and 10% acetic acid [85]. Gels were scanned
635 using a Cannon 5600F scanner for densitometric quantification.
636
637 **Protein Purification, Co-Precipitation, and Western Blotting**
638 dPINK1-His-V5 or dMIC60-His-V5 fusion protein was bacterially expressed, purified by a Ni-
639 NTA column, and eluted with elution buffer (50 mM $NaPO_4$, pH 8.0, 0.3 M NaCl, 250 mM
640 Imidazole). GST-dMIC60 fusion protein was bacterially expressed, purified and immobilized on
641 glutathione beads, and incubated with 5 μg dPINK1-His-V5 protein in NETN buffer (100 mM
642 NaCl, 20 mM Tris at pH 8.0, 0.5% NP40, 0.5 mM EDTA, and PMSF), at 4°C for 2 hrs [86]. Co-

643 precipitation complexes were then washed three times with NETN buffer. For *in vivo*
644 immunoprecipitation, mitochondrial fractions isolated from 100 pupae were lysed using NET-2
645 buffer (50 mM Tris-HCl, pH 7.5, 150 mM NaCl, 0.05% NP40) and incubated with 1 µl anti-
646 dMIC60 for 2 hrs at 4°C, and then 50 µl 50% washed protein A-Sepharose beads (Amersham)
647 for another 2 hrs at 4°C. The beads were then washed three times with NET-2 buffer. The
648 following antibodies were used: rabbit anti-V5 (E10/V4RR, Thermo) at 1:2000, rabbit anti-GST
649 (8-326, Thermo) at 1:2000, rabbit anti-dPINK1 (gift of Dr. Bingwei Lu) at 1:1000, rabbit anti-
650 dMIC60 at 1:6000, rabbit anti-phospho-dMIC60 at 1:5000, guinea pig anti-DMiro (GP5) [67] at
651 1:20000, rabbit anti-Flag (F7425; Sigma) at 1:2000, rabbit anti-OPA1–anti-human mitofusion 2,
652 which recognizes *Drosophila* OPA-1 [59]–(M6319; Sigma) at 1:1000, mouse anti-tubulin (T6199;
653 Sigma) at 1:3000, mouse anti-Myc (sc-40; Santa Cruz) at 1:1000, or mouse anti-ATP5α
654 (ab14748; AbCam) at 1:5000, and HRP-conjugated-goat anti-rabbit, guinea pig, or mouse IgG
655 (Jackson ImmunoResearch Laboratories) at 1:5000.
656
657 **TcPINK1 Kinase Assay**
658 TcPINK1 fused with maltose-binding protein (MBP) [55] was expressed in *E. coli*, purified using
659 amylose resin, and then eluted using kinase assay buffer containing maltose (50 mM Tris–HCl
660 pH 7.5, 0.1 mM EGTA, 10 mM $MgCl_2$, 2 mM dithiothreitol, and 10 mM maltose). Purified
661 TcPINK1 (1 µg) was then incubated with dMIC60-His-V5 (1 µg) in a final volume of 80 µl in
662 kinase assay buffer containing 10 mM ATP at 30°C for 2 hrs, and the reaction was terminated by
663 adding SDS sample buffer (300 mM Tris/HCl pH 6.8, 25% glycerol, 10% SDS, 0.1%
664 bromophenol blue, and 14.4 mM 2-mercaptoethanol). Reaction mixtures were resolved either in
665 7.5% SDS-PAGE then sent for mass spectrometric analysis (see below), or in 6% SDS-PAGE

containing 100 µM acrylamide-pendant phos-tag ligand and 100 µM $MnCl_2$ as instructed (http://www.wako-chem.co.jp/english/labchem/product/life/Phos-tag/Acrylamide.htm). Phos-tag containing SDS-PAGE was rinsed in transfer buffer with 1 mM EDTA for 10 min to remove Mn^{2+} before transfer. For time-course kinase assay, 0.1 nM purified TcPINK1 was incubated with 1 µM purified dMIC60-His-V5 or 1 µM ubiquitin (P0CG47; R&D Systems) in a final volume of 80 µl in kinase assay buffer containing 100 µM ATP (ADP free) for 0~60 min at 30°C. The reactions were then heat-inactivated (5 min at 95°C) to stop TcPINK1 kinase activity. Next, 25 µl reaction sample was incubated with 25 µl ADP-Glo reagent (V6930: Promega) at room temperature for 45 min to degrade residual ATP. ADP was then converted to ATP by adding 50 µl of ADP-Glo Reagent II. The newly synthesized ATP was measured using a luciferase/luciferin reaction. Luminescence was read after 30 min of incubation at room temperature, using a Glomax Multi Jr. Reader (Promega).

Mass Spectrometry

Gel bands were excised, cut to small pieces and transferred into microtubes. In-gel digestion was performed as described elsewhere [24]. Briefly, gel pieces were destained, and proteins were reduced and alkylated using dithiothreitol and acrylamide prior to trypsin digestion overnight. The next day, peptides were extracted from the gel pieces, dried using a vacuum centrifuge, desalted using C_{18} STAGE tips, dried again, and resuspended in 50 mM citrate [87]. For LC-MSMS analysis, an Easy-nLC 1000 ultra-high performance liquid chromatography system coupled to an Orbitrap Velos mass spectrometer (both Thermo Fisher Scientific, Bremen, Germany) was used. Analytical columns were self-packed with 5 µm ReproSil-Pur 120 C_{18}-AQ particles (Dr. Maisch, Ammerbuch-Entringen, Germany) using spray tips manufactured from

100 µm inner diameter fused silica capillaries using a P2000 laser puller (Sutter Instruments, Novato, CA, USA). After equilibrating the column with 3 injections of 50 mM citrate, peptide samples were loaded at 1 µl/min in 100% buffer A (water with 0.1% formic acid). After 5 min of washing with the same settings, peptides were eluted with a linear gradient from 100% buffer A to 65% buffer A 35% buffer B (acetonitrile with 0.1% formic acid) in 30 min at a flow rate of 400 nl/min. Eluting peptides were ionized in the positive ion mode using a capillary voltage of 1.6 kV. One survey scan of the intact peptide ions was performed in the Orbitrap part of the mass spectrometer at a resolution of 30,000 followed by MSMS fragmentation of the top 10 most abundant peptide ions in the ion trap part using multi stage activation. Dynamic exclusion was set to 30 sec with an exclusion list size of 250. For peptide identification, resulting raw files were processed using Proteome Discoverer 1.4.1. (Thermo Scientific) and searched against Swissprot_2014_01 (www.uniprot.org) and cRAP (www.thegpm.org/crap) using MASCOT 2.4.1. (www.matrixscience.com). Taxonomy was set to *Drosophila* and enzyme specificity to trypsin. Propionamide (cysteine) was selected as fixed modification, and phosphorylation (serine, threonine, and tyrosine) as well as oxidation (methionine) were selected as variable modifications. Mass errors were set to 10 ppm at the MS level and 0.6 Da at the MSMS level. Peptides were filtered at 1% false discovery rate and MSMS spectra of identified phopshopeptides were validated manually. For peptide quantification, extracted ion chromatograms (XICs) of the monoisotopic peak of the respective peptide species (phosphorylated peptides and their unmodified counterparts) were generated, the area under the curve was quantified using Xcalibur 2.2. (Thermo Scientific), and the data was further processed using Microsoft Excel.

712 **Transmission Electron Microscopy (TEM) and Immuno-Gold Labeling**

713 Dissected larvae and adult thoraces were fixed in modified Trump's fixative (0.1 M sodium
714 cacodylate buffer, 1% glutaraldehyde, and 4% formaldehyde) at room temperature (22°C) and
715 kept at 4°C overnight. The fixed specimens were rinsed three times with 0.1 M sodium
716 cacodylate pH 7.4 for 10 min, post-fixed with 0.1 M sodium cacodylate containing 2% osmium
717 tetroxide for 30 min, rinsed three times with 0.1 M sodium cacodylate for 10 min, and finally
718 rinsed five times with ddH_2O for 10 min. For Immuno-gold labeling, third instar larvae were
719 dissected in Schneider's medium with 5 mM EGTA and fixed by pre-fix solution (0.1%
720 glutaraldehyde, 0.1 M sodium cacodylate buffer, 4% formaldehyde, and 2 mM $MgCl_2$) for 1 hr at
721 room temperature. Samples were incubated with rabbit anti-Flag (1:100; F7425, Sigma)
722 overnight at 4°C, followed by incubation with anti-rabbit IgG 1.4-nm samples nanogold (1:50;
723 Nanoprobes) for 1 hr at room temperature and washes with ddH_2O. Samples were then postfixed
724 by Trump's fixative (0.1 M sodium cacodylate buffer, 1% glutaraldehyde, and 4% formaldehyde)
725 for 1 hr at 4°C. The specimens were stained en bloc in 2% aqueous uranyl acetate for 30 min,
726 dehydrated in a graded ethanol series, and subsequently set into Spurr's embedding medium.
727 Thin sections (90 nm) were stained with uranyl acetate and lead citrate, and imaged with a
728 TEM1230 electron microscope (JEOL Company) and a 967 slow-scan, cooled CCD camera
729 (Gatan). Muscles at the A4 segment were sectioned 90 nm apart for 10 consecutive sections
730 starting from the middle line. All sections were quantified for all genotypes. All EM images were
731 processed with Photoshop CS4.

732

733 **Behavior Assay**

734 Larval crawling ability was defined as the larva's ability to move from the center of a 55-mm

apple agar plate to halfway to the edge (13.75 mm) within 30 sec. Climbing ability was defined as the ability of the adult fly to climb 5 cm within 5 sec. Jumping ability was defined as the ability of the adult fly to respond to being tapped in a petri dish by jumping to right itself. Flying ability was defined as the ability to fly when the dish was turned upside down at 30 cm above a bench. If the fly could accomplish the task, it was given a score of 1; otherwise it was given a score of 0. The ability was quantified as a percentage of total flies that were scored a 1.

Human Cell Culture and TEM

Human iPSC-derived neurons from a healthy subject (XK-001-1V) and the corresponding isogenic *PINK1-/-* neurons (XK-001-ZOC-B-1V) were purchased from the XCell Science (http://xcell2.com/products-2/ipsc%20lines/isogenic%20knockout%20lines.html). The genotypes, gene expression levels, pluripotency, and neuronal identity of these iPSCs and neurons were fully validated by XCell Science. Partially differentiated neurons (7 days *in vitro*) were further differentiated on poly-ornithine and laminin coated Thermanox coverslips (77280; EMS) in a 24-well plate, using Neuro Maturation Media (XCell Science: NM-001-M50) and supplement A (NM-SA) for additional 8 days. This allows more than 90% Tuj1-positive neuronal population according to the manufacture's instruction. HEK293T cells cultured on poly-ornithine and laminin coated Thermanox coverslips were transfected with respective siRNA and RNAi-resistant constructs using calcium phosphate. For MIC60 RNAi, silencer validated siRNA (targeting CACCCAAGCUUUAACCGCATT; S21634, Thermo Fisher Scientific) was applied. A non-targeting siRNA (SIC001, Sigma-Aldrich) with no known mammalian homology was used as a negative control. MIC60 RNAi-resistant pcDNA3.1-MIC60-Myc was generated by substituting the MIC60 RNAi-targeting sequence–CACCCAAGCTTTAACCGCA–with

TACACAGGCATTGACTGCA. After transfection for 2 days, cells were fixed for TEM or lysed for western blotting. Neurons and HEK293T cells were fixed with 2% glutaraldehyde and 4% paraformaldehyde in 0.1 M Sodium Cacodylate buffer, pH 7.4 at 4°C overnight. Sample preparation for TEM was performed as described above.

Human Genetics

For the Taiwanese cohort, 1883 study participants including 250 sporadic early-onset PD patients (onset age<50 years), 602 sporadic late-onset PD patients (onset age≥50 years), 100 familial PD patients with positive family history (at least one other affected first- and/or second-degree relative with parkinsonism), and 931 age/gender/ethnicity-matched controls, were recruited from the movement disorder clinic of the National Taiwan University Hospital, a tertiary referral center in Taiwan. Among the 100 familial PD patients, 43 followed an autosomal-dominant inheritance pattern, 23 showed autosomal-recessive inheritance, and the remaining 34 had one affected second-degree relative. PD was diagnosed using the UK PD Society Brain Bank diagnostic criteria [88]. Unrelated healthy adult volunteers matched for age, gender, and ethnic origins were recruited as controls. Informed consent was obtained from each participant, and the institutional ethics board committees approved this study. DNA extraction from venous blood was performed using standard protocols [89]. In the first part of the study, complete Sanger sequencing of all the exons and exon-intron boundaries of *MIC60* gene was performed in 250 sporadic early-onset PD patients, 100 probands with positive family history, and 350 age/gender/ethnicity-matched controls. The 15 exons and exon-intron boundaries of *MIC60* gene were amplified using PCR and sequenced by an ABI 3730 analyzer (Applied Biosystems Inc). The primer sequences are provided in Supplementary Table 1. The multiple

ligation probe amplification (MLPA) kits P051 and P052 (MRC Holland, Amsterdam, The Netherlands), covering the exons of *SNCA*, *Parkin*, *PINK1*, *DJ-1*, *ATP13A2*, *PLA2G6*, *FBXO7*, or *DNAJC6*, were used to screen for these genes known to cause early-onset familial parkinsonism. Detection of *LRRK2* mutations was described previously [89]. For the second set of the study, we genotyped the potential pathogenic *c.G50T* (p.Cys17Phe) substitution using TaqMan® Genotyping Assays on a StepOnePlus Real-Time PCR machine (Applied Biosystems Inc) in additional 602 sporadic late-onset PD patients and additional 581 age/gender/ethnicity-matched control subjects. In the first part of the study including 250 sporadic early-onset and 100 probands of familial PD patients, the age of symptomatic onset was 51.3±15.3 years (range, 35–74 years for 203 men and 147 women). In the second part including additional 602 sporadic late-onset PD patients, the onset age was 63.4±7.9 years and 51.2% are men. Both patients with the *MIC60 c.G50T* mutation are clinically late-onset. The male familial patient first had progressive asymmetrical rest tremor and slow movement at the age of 61 and has responded well to levodopa for 7 years since onset. The UPDRS part III score was improved from 25 to 8 using levodopa at a dose of 600 mg/day. The male sporadic patient first had motor symptoms at the age of 67 and responded well to levodopa. He developed dementia 7 years after motor symptom onset and the MMSE score was 21/30. His head MRI shows diffuse cortical atrophy with slight emphasis on the frontal cortices (Supplementary Fig. 11).

The Mayo Clinic PD patient-control cohort consisted of 859 PD patients (age = 76.69±11.11 years) [68, 90]. The age of symptomatic onset was 65.50±13.08 years (range, 28–97 years for 546 men and 313 women). A family history was noted in 352 patients and 115 patients presented with early-onset form of the disease (defined as symptomatic onset ≤50 years). The study included 871 healthy controls (age = 65.08±12.74 years for 374 men and 497 women with no

804 family history of neurodegenerative movement disorder). All subjects included in the study are
805 unrelated, non-Hispanic Caucasians recruited at Mayo Clinic, Jacksonville. Both patients
806 harboring the *MIC60* MTS mutants (p.A4V and p.R25H) are late-onset sporadic patients with no
807 recorded family history of the disease.

808 PPMI is an international, multi-center and progressing study designed to identify PD
809 biomarkers by the Michael J. Fox Foundation (http://www.ppmi-info.org/study-design/). The
810 study design, subject recruitment criteria, site selection, and study assessment have been detailed
811 in [69].

812

813 **Statistical Analysis**

814 Throughout the paper, the distribution of data points is expressed as box-whisker plots, except
815 otherwise stated. The One-Way ANOVA Post-Hoc Tukey test was performed for comparisons
816 among multiple groups. The Mann-Whitney *U* test was performed for comparisons between two
817 groups. The Chi Square Test was performed for behavioral tests. Statistical tests were performed
818 using SPSS.

819

820 # REFERENCES

821

822 1. Mannella, C.A., Lederer, W.J. & Jafri, M.S. The connection between inner membrane
823 topology and mitochondrial function. *Journal of molecular and cellular cardiology* **62**, 51-57
824 (2013).
825 2. Harner, M.*, et al.* The mitochondrial contact site complex, a determinant of mitochondrial
826 architecture. *The EMBO journal* **30**, 4356-4370 (2011).
827 3. Hoppins, S.*, et al.* A mitochondrial-focused genetic interaction map reveals a scaffold-
828 like complex required for inner membrane organization in mitochondria. *The Journal of cell*
829 *biology* **195**, 323-340 (2011).
830 4. Rabl, R.*, et al.* Formation of cristae and crista junctions in mitochondria depends on
831 antagonism between Fcj1 and Su e/g. *The Journal of cell biology* **185**, 1047-1063 (2009).
832 5. von der Malsburg, K.*, et al.* Dual role of mitofilin in mitochondrial membrane
833 organization and protein biogenesis. *Developmental cell* **21**, 694-707 (2011).

6. Zerbes, R.M., *et al.* Mitofilin complexes: conserved organizers of mitochondrial membrane architecture. *Biological chemistry* **393**, 1247-1261 (2012).
7. van der Laan, M., Bohnert, M., Wiedemann, N. & Pfanner, N. Role of MINOS in mitochondrial membrane architecture and biogenesis. *Trends in cell biology* **22**, 185-192 (2012).
8. Messerschmitt, M., *et al.* The inner membrane protein Mdm33 controls mitochondrial morphology in yeast. *The Journal of cell biology* **160**, 553-564 (2003).
9. Frezza, C., *et al.* OPA1 controls apoptotic cristae remodeling independently from mitochondrial fusion. *Cell* **126**, 177-189 (2006).
10. Meeusen, S., *et al.* Mitochondrial inner-membrane fusion and crista maintenance requires the dynamin-related GTPase Mgm1. *Cell* **127**, 383-395 (2006).
11. Strauss, M., Hofhaus, G., Schroder, R.R. & Kuhlbrandt, W. Dimer ribbons of ATP synthase shape the inner mitochondrial membrane. *The EMBO journal* **27**, 1154-1160 (2008).
12. Mannella, C.A. Structure and dynamics of the mitochondrial inner membrane cristae. *Biochimica et biophysica acta* **1763**, 542-548 (2006).
13. Mannella, C.A., Marko, M., Penczek, P., Barnard, D. & Frank, J. The internal compartmentation of rat-liver mitochondria: tomographic study using the high-voltage transmission electron microscope. *Microscopy research and technique* **27**, 278-283 (1994).
14. Mannella, C.A., Buttle, K., Rath, B.K. & Marko, M. Electron microscopic tomography of rat-liver mitochondria and their interaction with the endoplasmic reticulum. *BioFactors* **8**, 225-228 (1998).
15. Khalifat, N., Puff, N., Bonneau, S., Fournier, J.B. & Angelova, M.I. Membrane deformation under local pH gradient: mimicking mitochondrial cristae dynamics. *Biophysical journal* **95**, 4924-4933 (2008).
16. John, G.B., *et al.* The mitochondrial inner membrane protein mitofilin controls cristae morphology. *Molecular biology of the cell* **16**, 1543-1554 (2005).
17. Hackenbrock, C.R. Ultrastructural bases for metabolically linked mechanical activity in mitochondria. I. Reversible ultrastructural changes with change in metabolic steady state in isolated liver mitochondria. *The Journal of cell biology* **30**, 269-297 (1966).
18. Valente, E.M., *et al.* Hereditary early-onset Parkinson's disease caused by mutations in PINK1. *Science* **304**, 1158-1160 (2004).
19. Silvestri, L., *et al.* Mitochondrial import and enzymatic activity of PINK1 mutants associated to recessive parkinsonism. *Human molecular genetics* **14**, 3477-3492 (2005).
20. Jin, S.M., *et al.* Mitochondrial membrane potential regulates PINK1 import and proteolytic destabilization by PARL. *The Journal of cell biology* **191**, 933-942 (2010).
21. Greene, A.W., *et al.* Mitochondrial processing peptidase regulates PINK1 processing, import and Parkin recruitment. *EMBO reports* **13**, 378-385 (2012).
22. Morais, V.A., *et al.* PINK1 loss-of-function mutations affect mitochondrial complex I activity via NdufA10 ubiquinone uncoupling. *Science* **344**, 203-207 (2014).
23. Thomas, R.E., Andrews, L.A., Burman, J.L., Lin, W.Y. & Pallanck, L.J. PINK1-Parkin pathway activity is regulated by degradation of PINK1 in the mitochondrial matrix. *PLoS genetics* **10**, e1004279 (2014).
24. Wang, X., *et al.* PINK1 and Parkin target Miro for phosphorylation and degradation to arrest mitochondrial motility. *Cell* **147**, 893-906 (2011).
25. Narendra, D., Walker, J.E. & Youle, R. Mitochondrial quality control mediated by PINK1 and Parkin: links to parkinsonism. *Cold Spring Harbor perspectives in biology* **4** (2012).
26. Zhou, C., *et al.* The kinase domain of mitochondrial PINK1 faces the cytoplasm.

Proceedings of the National Academy of Sciences of the United States of America **105**, 12022-12027 (2008).
27. Geisler, S.*, et al.* PINK1/Parkin-mediated mitophagy is dependent on VDAC1 and p62/SQSTM1. *Nature cell biology* **12**, 119-131 (2010).
28. Narendra, D., Tanaka, A., Suen, D.F. & Youle, R.J. Parkin is recruited selectively to impaired mitochondria and promotes their autophagy. *The Journal of cell biology* **183**, 795-803 (2008).
29. Vives-Bauza, C. & Przedborski, S. Mitophagy: the latest problem for Parkinson's disease. *Trends in molecular medicine* **17**, 158-165 (2011).
30. Whitworth, A.J. & Pallanck, L.J. The PINK1/Parkin pathway: a mitochondrial quality control system? *Journal of bioenergetics and biomembranes* **41**, 499-503 (2009).
31. Kane, L.A.*, et al.* PINK1 phosphorylates ubiquitin to activate Parkin E3 ubiquitin ligase activity. *The Journal of cell biology* **205**, 143-153 (2014).
32. Koyano, F.*, et al.* Ubiquitin is phosphorylated by PINK1 to activate parkin. *Nature* **510**, 162-166 (2014).
33. Kazlauskaite, A.*, et al.* Parkin is activated by PINK1-dependent phosphorylation of ubiquitin at Ser65. *The Biochemical journal* **460**, 127-139 (2014).
34. Chen, Y. & Dorn, G.W., 2nd. PINK1-phosphorylated mitofusin 2 is a Parkin receptor for culling damaged mitochondria. *Science* **340**, 471-475 (2013).
35. Kondapalli, C.*, et al.* PINK1 is activated by mitochondrial membrane potential depolarization and stimulates Parkin E3 ligase activity by phosphorylating Serine 65. *Open biology* **2**, 120080 (2012).
36. Pogson, J.H.*, et al.* The complex I subunit NDUFA10 selectively rescues Drosophila pink1 mutants through a mechanism independent of mitophagy. *PLoS genetics* **10**, e1004815 (2014).
37. Vilain, S.*, et al.* The yeast complex I equivalent NADH dehydrogenase rescues pink1 mutants. *PLoS genetics* **8**, e1002456 (2012).
38. Vos, M.*, et al.* Vitamin K2 is a mitochondrial electron carrier that rescues pink1 deficiency. *Science* **336**, 1306-1310 (2012).
39. Gehrke, S.*, et al.* PINK1 and Parkin control localized translation of respiratory chain component mRNAs on mitochondria outer membrane. *Cell metabolism* **21**, 95-108 (2015).
40. Liu, W.*, et al.* Pink1 regulates the oxidative phosphorylation machinery via mitochondrial fission. *Proceedings of the National Academy of Sciences of the United States of America* **108**, 12920-12924 (2011).
41. Clark, I.E.*, et al.* Drosophila pink1 is required for mitochondrial function and interacts genetically with parkin. *Nature* **441**, 1162-1166 (2006).
42. Attwell, D. & Laughlin, S.B. An energy budget for signaling in the grey matter of the brain. *Journal of cerebral blood flow and metabolism : official journal of the International Society of Cerebral Blood Flow and Metabolism* **21**, 1133-1145 (2001).
43. Lajtha, A., Gibson, G.E. & Dienel, G.A. *Handbook of Neurochemistry and Molecular Neurobiology: Brain Energetics. Integration of Molecular and Cellular Processes* (Springer, 2007).
44. Weihofen, A., Thomas, K.J., Ostaszewski, B.L., Cookson, M.R. & Selkoe, D.J. Pink1 forms a multiprotein complex with Miro and Milton, linking Pink1 function to mitochondrial trafficking. *Biochemistry* **48**, 2045-2052 (2009).
45. Markstein, M., Pitsouli, C., Villalta, C., Celniker, S.E. & Perrimon, N. Exploiting position

effects and the gypsy retrovirus insulator to engineer precisely expressed transgenes. *Nature genetics* **40**, 476-483 (2008).
46. Park, J.*, et al.* Mitochondrial dysfunction in Drosophila PINK1 mutants is complemented by parkin. *Nature* **441**, 1157-1161 (2006).
47. Greene, J.C.*, et al.* Mitochondrial pathology and apoptotic muscle degeneration in Drosophila parkin mutants. *Proceedings of the National Academy of Sciences of the United States of America* **100**, 4078-4083 (2003).
48. Pesah, Y.*, et al.* Drosophila parkin mutants have decreased mass and cell size and increased sensitivity to oxygen radical stress. *Development* **131**, 2183-2194 (2004).
49. Exner, N.*, et al.* Loss-of-function of human PINK1 results in mitochondrial pathology and can be rescued by parkin. *The Journal of neuroscience : the official journal of the Society for Neuroscience* **27**, 12413-12418 (2007).
50. Alkhaja, A.K.*, et al.* MINOS1 is a conserved component of mitofilin complexes and required for mitochondrial function and cristae organization. *Molecular biology of the cell* **23**, 247-257 (2012).
51. Xie, J., Marusich, M.F., Souda, P., Whitelegge, J. & Capaldi, R.A. The mitochondrial inner membrane protein mitofilin exists as a complex with SAM50, metaxins 1 and 2, coiled-coil-helix coiled-coil-helix domain-containing protein 3 and 6 and DnaJC11. *FEBS letters* **581**, 3545-3549 (2007).
52. Herrmann, J.M. MINOS is plus: a Mitofilin complex for mitochondrial membrane contacts. *Developmental cell* **21**, 599-600 (2011).
53. Itoh, K., Tamura, Y., Iijima, M. & Sesaki, H. Effects of Fcj1-Mos1 and mitochondrial division on aggregation of mitochondrial DNA nucleoids and organelle morphology. *Molecular biology of the cell* **24**, 1842-1851 (2013).
54. Korner, C.*, et al.* The C-terminal domain of Fcj1 is required for formation of crista junctions and interacts with the TOB/SAM complex in mitochondria. *Molecular biology of the cell* **23**, 2143-2155 (2012).
55. Woodroof, H.I.*, et al.* Discovery of catalytically active orthologues of the Parkinson's disease kinase PINK1: analysis of substrate specificity and impact of mutations. *Open biology* **1**, 110012 (2011).
56. Schuldiner, O.*, et al.* piggyBac-based mosaic screen identifies a postmitotic function for cohesin in regulating developmental axon pruning. *Developmental cell* **14**, 227-238 (2008).
57. Yang, Y.*, et al.* Pink1 regulates mitochondrial dynamics through interaction with the fission/fusion machinery. *Proceedings of the National Academy of Sciences of the United States of America* **105**, 7070-7075 (2008).
58. Poole, A.C.*, et al.* The PINK1/Parkin pathway regulates mitochondrial morphology. *Proceedings of the National Academy of Sciences of the United States of America* **105**, 1638-1643 (2008).
59. Poole, A.C., Thomas, R.E., Yu, S., Vincow, E.S. & Pallanck, L. The mitochondrial fusion-promoting factor mitofusin is a substrate of the PINK1/parkin pathway. *PloS one* **5**, e10054 (2010).
60. Ziviani, E., Tao, R.N. & Whitworth, A.J. Drosophila parkin requires PINK1 for mitochondrial translocation and ubiquitinates mitofusin. *Proceedings of the National Academy of Sciences of the United States of America* **107**, 5018-5023 (2010).
61. Yun, J.*, et al.* MUL1 acts in parallel to the PINK1/parkin pathway in regulating mitofusin and compensates for loss of PINK1/parkin. *eLife* **3**, e01958 (2014).

62. Mun, J.Y., *et al.* Caenorhabditis elegans mitofilin homologs control the morphology of mitochondrial cristae and influence reproduction and physiology. *Journal of cellular physiology* **224**, 748-756 (2010).
63. Yang, Y., *et al.* Mitochondrial pathology and muscle and dopaminergic neuron degeneration caused by inactivation of Drosophila Pink1 is rescued by Parkin. *Proceedings of the National Academy of Sciences of the United States of America* **103**, 10793-10798 (2006).
64. Zick, M., Rabl, R. & Reichert, A.S. Cristae formation-linking ultrastructure and function of mitochondria. *Biochimica et biophysica acta* **1793**, 5-19 (2009).
65. Gegg, M.E., Cooper, J.M., Schapira, A.H. & Taanman, J.W. Silencing of PINK1 expression affects mitochondrial DNA and oxidative phosphorylation in dopaminergic cells. *PloS one* **4**, e4756 (2009).
66. Gispert, S., *et al.* Parkinson phenotype in aged PINK1-deficient mice is accompanied by progressive mitochondrial dysfunction in absence of neurodegeneration. *PloS one* **4**, e5777 (2009).
67. Tsai, P.I., *et al.* PINK1-mediated phosphorylation of Miro inhibits synaptic growth and protects dopaminergic neurons in Drosophila. *Scientific reports* **4**, 6962 (2014).
68. Ogaki, K., *et al.* Mitochondrial targeting sequence variants of the CHCHD2 gene are a risk for Lewy body disorders. *Neurology* **85**, 2016-2025 (2015).
69. Parkinson Progression Marker, I. The Parkinson Progression Marker Initiative (PPMI). *Progress in neurobiology* **95**, 629-635 (2011).
70. Jansen, I.E., *et al.* Discovery and functional prioritization of Parkinson's disease candidate genes from large-scale whole exome sequencing. *Genome Biol* **18**, 22 (2017).
71. Schork, N.J., Murray, S.S., Frazer, K.A. & Topol, E.J. Common vs. rare allele hypotheses for complex diseases. *Curr Opin Genet Dev* **19**, 212-219 (2009).
72. Song, S., *et al.* Characterization of PINK1 (PTEN-induced putative kinase 1) mutations associated with Parkinson disease in mammalian cells and Drosophila. *The Journal of biological chemistry* **288**, 5660-5672 (2013).
73. Lai, Y.C., *et al.* Phosphoproteomic screening identifies Rab GTPases as novel downstream targets of PINK1. *The EMBO journal* **34**, 2840-2861 (2015).
74. Sim, C.H., Gabriel, K., Mills, R.D., Culvenor, J.G. & Cheng, H.C. Analysis of the regulatory and catalytic domains of PTEN-induced kinase-1 (PINK1). *Human mutation* **33**, 1408-1422 (2012).
75. Akabane, S., *et al.* PKA Regulates PINK1 Stability and Parkin Recruitment to Damaged Mitochondria through Phosphorylation of MIC60. *Molecular cell* **62**, 371-384 (2016).
76. Dagda, R.K., *et al.* Mitochondrially localized PKA reverses mitochondrial pathology and dysfunction in a cellular model of Parkinson's disease. *Cell death and differentiation* **18**, 1914-1923 (2011).
77. Dagda, R.K., *et al.* Beyond the mitochondrion: cytosolic PINK1 remodels dendrites through protein kinase A. *Journal of neurochemistry* **128**, 864-877 (2014).
78. Silvestri, E., *et al.* Thyroid-hormone effects on putative biochemical pathways involved in UCP3 activation in rat skeletal muscle mitochondria. *FEBS letters* **579**, 1639-1645 (2005).
79. Surmeier, D.J., Guzman, J.N. & Sanchez-Padilla, J. Calcium, cellular aging, and selective neuronal vulnerability in Parkinson's disease. *Cell calcium* **47**, 175-182 (2010).
80. Ryan, B.J., Hoek, S., Fon, E.A. & Wade-Martins, R. Mitochondrial dysfunction and mitophagy in Parkinson's: from familial to sporadic disease. *Trends in biochemical sciences* **40**, 200-210 (2015).

81. Pacelli, C.*, et al.* Elevated Mitochondrial Bioenergetics and Axonal Arborization Size Are Key Contributors to the Vulnerability of Dopamine Neurons. *Current biology : CB* **25**, 2349-2360 (2015).
82. Groth, A.C., Fish, M., Nusse, R. & Calos, M.P. Construction of transgenic Drosophila by using the site-specific integrase from phage phiC31. *Genetics* **166**, 1775-1782 (2004).
83. Park, Y.U.*, et al.* Disrupted-in-schizophrenia 1 (DISC1) plays essential roles in mitochondria in collaboration with Mitofilin. *Proceedings of the National Academy of Sciences of the United States of America* **107**, 17785-17790 (2010).
84. Shidara, Y. & Hollenbeck, P.J. Defects in mitochondrial axonal transport and membrane potential without increased reactive oxygen species production in a Drosophila model of Friedreich ataxia. *The Journal of neuroscience : the official journal of the Society for Neuroscience* **30**, 11369-11378 (2010).
85. Wittig, I., Karas, M. & Schagger, H. High resolution clear native electrophoresis for in-gel functional assays and fluorescence studies of membrane protein complexes. *Molecular & cellular proteomics : MCP* **6**, 1215-1225 (2007).
86. Tsai, P.I.*, et al.* Neurofibromin mediates FAK signaling in confining synapse growth at Drosophila neuromuscular junctions. *The Journal of neuroscience : the official journal of the Society for Neuroscience* **32**, 16971-16981 (2012).
87. Winter, D., Seidler, J., Ziv, Y., Shiloh, Y. & Lehmann, W.D. Citrate boosts the performance of phosphopeptide analysis by UPLC-ESI-MS/MS. *Journal of proteome research* **8**, 418-424 (2009).
88. Hughes, A.J., Daniel, S.E., Kilford, L. & Lees, A.J. Accuracy of clinical diagnosis of idiopathic Parkinson's disease: a clinico-pathological study of 100 cases. *Journal of neurology, neurosurgery, and psychiatry* **55**, 181-184 (1992).
89. Lin, C.H.*, et al.* LRRK2 mutation in familial Parkinson's disease in a Taiwanese population: clinical, PET, and functional studies. *Journal of biomedical science* **15**, 661-667 (2008).
90. Puschmann, A.*, et al.* Heterozygous PINK1 p.G411S increases risk of Parkinson's disease via a dominant-negative mechanism. *Brain : a journal of neurology* **140**, 98-117 (2017).

FIGURE LEGENDS

Figure 1. PINK1 Maintains Crista Junctions. (a) Cartoon depicting a mitochondrial crista junction (red circle). (b, f) TEM images of thin sections, performed on body wall muscles of late third instar larvae (120 hrs AEL). (c, f) Quantification of the percentage of total mitochondria per image that are normal, “onion”-like, “vacuole”-like, “dumbbell”-like, or “other” (abnormal mitochondria that do not belong to any of the aforementioned-categories). n=307-916 mitochondria from 32-98 images obtained from 6-8 flies. (d) Quantification of the number of crista junctions (where the crista membrane connects to the inner boundary membrane)

normalized to the length of the mitochondrial circumference. n=30 mitochondria from 30 images from 6-8 flies. (e) Schematic representation of PINK1-mediated energy need-dependent plasticity of crista structure in third instar larvae. In low energetic cells such as larval axons, neuronal cell bodies and NMJs, PINK1 is not required to form crista junctions. In high energetic cells such as larval muscles and neuropils, PINK1 is activated to maintain the growing number of crista junctions. Scale bars: 500 nm. WT: wild-type. ***PINK1^{null}***: *PINK1^{5}/Y; da-GAL4* [41]. ***Wild-type:*** *PE704/Y* (precise excision control males for *PINK1^{5}/Y*) [41]. ***PINK1^{null},da>PINK1$^{WT/\Delta MTS}$:*** *PINK1^{5}/Y;UAS-hPINK1$^{WT/\Delta MTS}$-Flag;da-GAL4.* ***Parkin^{null}***: *Park^{25};* ***Parkin^{RV}***: *Park^{rva}* [47]. Genotypes are written in the same way here and for all figures except otherwise stated. Comparisons with "*Wild-type*". * P<0.05, ** P<0.01, *** P<0.001, and the box-whisker plots are used for all figures unless otherwise stated.

Figure 2. PINK1 Interacts with and Phosphorylates dMIC60. (a) Immunoprecipitations with anti-dMIC60 were performed using the mitochondrial fractions of pupae 72 hrs After Pupa Formation (APF) with the indicated genotypes. (b) Schematic representation of the truncated GST-dMIC60 used in *in vitro* co-precipitation with glutathione beads and dPINK1-His-V5. FL: full length. Samples were immunoblotted as indicated. (c) Sequence alignments between the flanking regions of the two Threonine sites in dMIC60, or between the phospho-peptides of dMIC60 and human Miro1/2. (d) The upper blot is the phos-tag gel immunoblotted with anti-V5 in reactions as indicated. The lower blot is the Coomassie-stained gel revealing the proteins in the reactions. (e) Time-course analysis of *in vitro* TcPINK1 kinase phosphorylation of either dMIC60-His-V5 or ubiquitin using the ADP-Glo Kinase assay/luminescence detection system. (f-g) Left in (f): *in vitro* phosphorylation reactions as in (d) immunoblotted as indicated. Right

and bottom in (f), and (g): lysates of adults 5 days after eclosion were immunoblotted as indicated, and the band intensities of phospho-dMIC60 are normalized to those of total dMIC60. n=3 independent experiments. Comparisons with "*Wild-type*" (f) or "*PINK1*^{null}" (g).

Figure 3. PINK1-Mediated Phosphorylation of dMIC60 Maintains Crista Junctions. (a) TEM images of thin sections, performed on body wall muscles, VNC, NMJs, or segmental nerves of late third instar larvae (120 hrs AEL). Scale bars: 100 nm. (b) Quantification of the number of crista junctions normalized to the length of the mitochondrial circumference. n=30 mitochondria from 30 images obtained from 4-6 flies. (c) Quantification of the percentage of total mitochondria per image that are "onion-like". n=17-236 mitochondria from 8-15 images from 4-6 larvae. Bar graphs and mean±S.E.M are shown due to lack of variations of data at most data points. ***Wild-type***: *w*^{1118}. ***dMIC60*^{mut}*:*** *Tubulin-GAL4_dMIC60*$^{LL02849/LL02849}$. ***dMIC60*^{mut}*,dMIC60*$^{WT/PR}$*:*** *UAS-dMIC60-Myc*$^{WT/PR}$*;Tubulin-GAL4_dMIC60*$^{LL02849/LL02849}$. Genotypes are written in the same way here and for all figures except otherwise stated. Comparisons with "*Wild-type*".

Figure 4. MIC60 Restores Crista Structure of *PINK1* Null. (a-c) TEM images of thin sections, performed on body wall muscles of late third instar larvae (120 hrs AEL). Quantifications are performed as described in Figure 1. Tub: Tubulin-GAL4. n=219-371 mitochondria from 27-32 images obtained from 4-6 flies. Comparisons with the control group to the left. Scale bars: 500 nm. (d) Schematic representation of the differing mechanisms between larvae and adults by which PINK1 maintains crista structure. In larval muscles, PINK1-mediated phosphorylation of

MIC60 is required for maintaining crista structure. In adult thoracic muscles, multiple PINK1-mediated pathways are involved.

Figure 5. Both Phosphorylation and Overexpression of MIC60 Stabilize MIC60 Oligomerization. (a) BN-PAGE was immunoblotted with anti-V5 containing samples from the *in vitro* PINK1 phosphorylation reactions as indicated. (b) dMIC60 or phosphorylated dMIC60 was immunodetected in whole body lysates of 5-day-old adults as indicated, using either BN-PAGE or regular-PAGE. dMIC60 migrates as a tetramer or oligomerizes with other proteins based on the size in BN-PAGE. The same results were observed for 3 times. (c) Schematic representation of the potential impact of PINK1-mediated phosphorylation or overexpression of MIC60 on MIC60 oligomerization and crista curvatures. (d) The in-gel activity of complex I was measured. The representative blue-native gel and quantification of the band intensities compared to "*PINK1*^{null}*, da-GAL4*", are shown. n=100 adults 5 days after eclosion for each experiment and total 4 independent experiments.

Figure 6. MIC60 Restores the ATP level and ΔΨm, and Rescues the Behavioral Defects and DA Neurodegeneration in *PINK1* Null. (a) Quantification of the total ATP level in adult flies 5 days after eclosion. n=5 adults for each experiment and total 6 independent experiments. (b) Quantification of the mitochondrial/cytoplasmic TMRM fluorescent intensity in body wall muscles of third instar larvae. n=6 larvae. (c-f) The crawling ability of third instar larvae (c), and the climbing (d), jumping (e), and flying (f) abilities of adult flies 5 days after eclosion, were quantified. n=20-60 flies. The percentage of flies that are scored as a "1" (able to do it) is shown in black/gray bars, and the percentage of flies that are scored as a "0" (unable to do it) is shown

in white bars. The Chi Square Test is used as the data is categorical. For (a-f), ***Wild-type:*** *PE704/Y*. (g) The PPL1 clusters of DA neurons visualized by anti-TH in adult brains 15 days after eclosion. ***PINK1^{null}***: *PINK1^{B9}/Y* [46]. ***Wild-type:*** *PINK1^{RV}/Y* (precise excision control males for *PINK1^{B9}/Y*) [46]. *PINK1^{B9}/Y* exhibits the same crista impairments as *PINK1^{5}/Y* used in the other figures (Supplementary Fig. 3). (h) Quantification of the DA neuron number in one PPL1 or one PPL2 cluster per brain of adult flies 15 days after eclosion. n=10-14 brains. Genotypes are the same as in (g). For all panels, comparisons with "*PINK1^{null}, da-GAL4*". Scale bar: 5 μm.

Figure 7. *MIC60* Variants in Humans and *Drosophila*. (a) Depiction of the *MIC60* MTS variants identified in this study. (b) Viability analysis. One hundred late third instar larvae of each genotype were collected and the numbers of their pupae and adults were subsequently counted. (c) The crawling ability of third instar larvae with genotypes as indicated. n=20 larvae. The percentage of flies that are scored as a "1" is shown in black/color bars and the percentage of flies that are scored as a "0" is shown in white bars. The Chi Square Test is used. (d) Quantification of TEM images of thin sections performed on body wall muscles of late third instar larvae (120 hrs AEL) (representative images in Supplementary Fig. 11f) is performed as described in Figure 1. n=20 images from 6 flies. (e) Single sections of confocal images of immunostaining against endogenous dMIC60 (green) or exogenously expressed human MIC60-Myc (blue/white) on body wall muscles of third instar larvae. Red is the mitochondrial marker ATP5β. Note that anti-dMIC60 doesn't recognize expressed human MIC60. White arrow heads show colocalization between endogenous dMIC60 and ATP5β. Scale bar: 5 μm. Quantification of the percentage of ATP5β puncta that are also positive for dMIC60 or MIC60-Myc. n=12 images from 4-6 larvae. (c, d, e) Comparisons with "*Actin-GAL4;dMIC60^{mut}/+*" except indicated

otherwise. (f) Schematic representation of the potential mechanism underlying energy need-dependent plasticity of crista junctions in third instar larvae. In low energetic cells, unphosphorylated MIC60 is sufficient to form crista junctions. In high-energy cells, PINK1 is activated to phosphorylate MIC60 for maintaining of the increasing number of crista junctions.

a

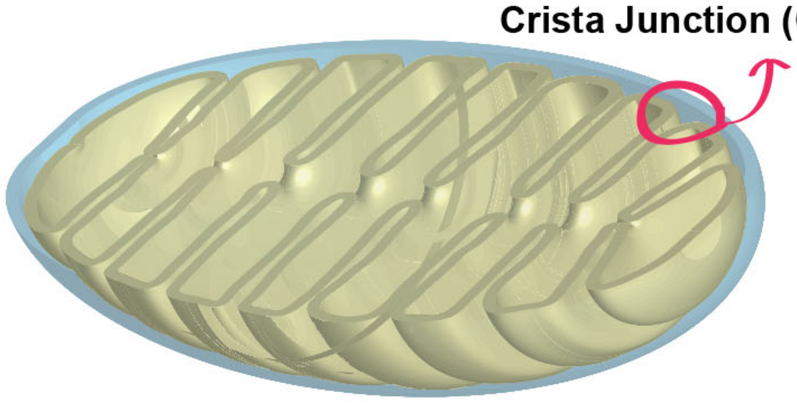
Crista Junction (CJ)

b

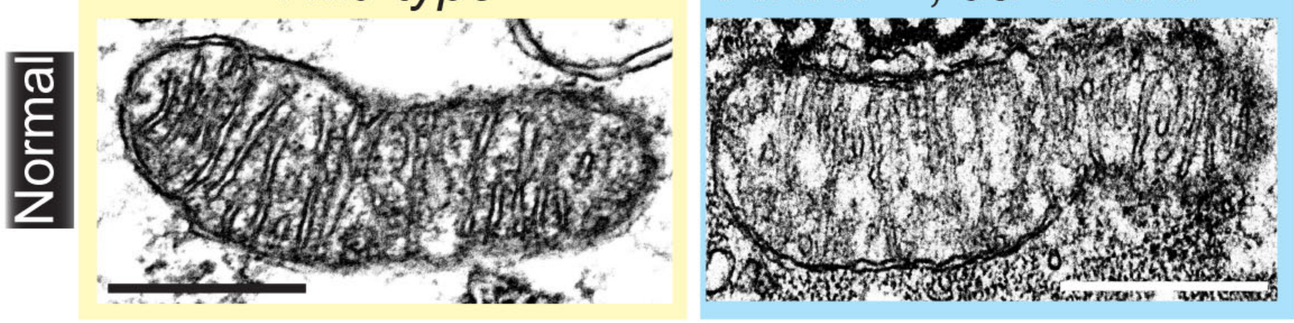
Late Third Instar Larval Body Wall Muscles
Wild-type
PINK1null, da>PINK1WT
Normal

c

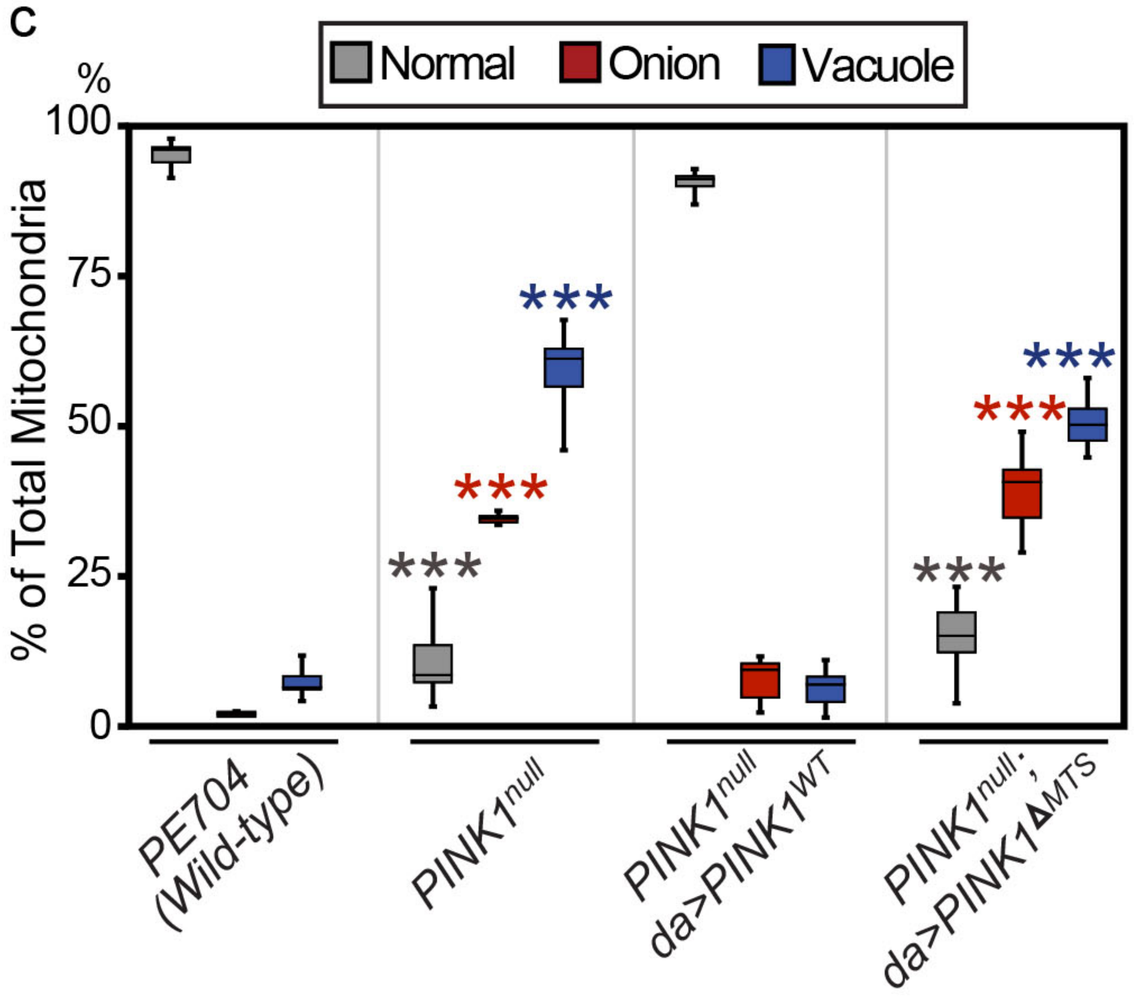
Normal
Onion
Vacuole
% of Total Mitochondria
100
75
50
25
0
***
PE704 (Wild-type)
PINK1null
PINK1null da>PINK1WT
PINK1null; da>PINK1ΔMTS

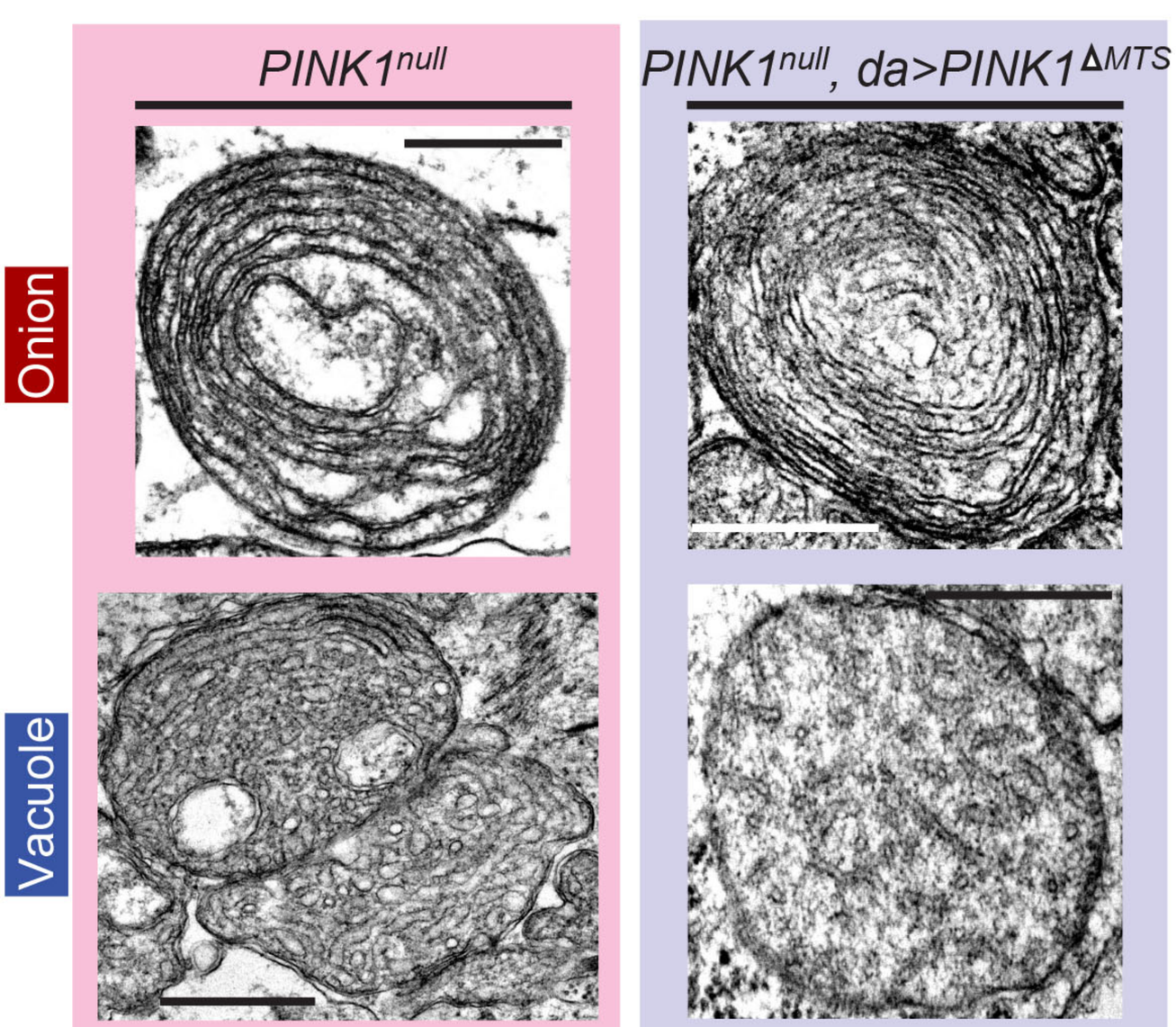
PINK1null
PINK1null, da>PINK1ΔMTS
Onion
Vacuole

d

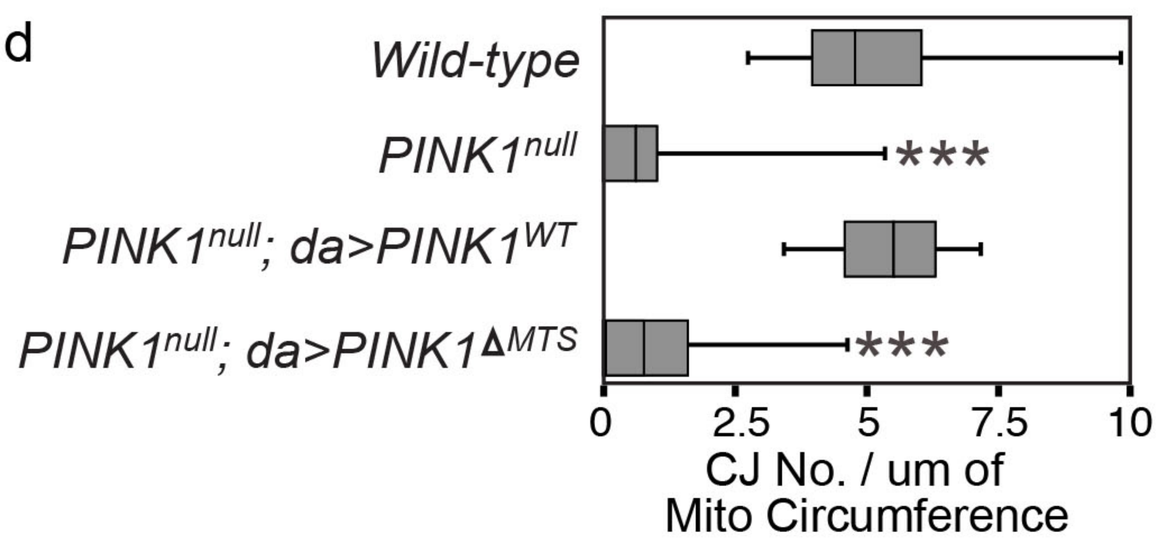
Wild-type
PINK1null
PINK1null; da>PINK1WT
PINK1null; da>PINK1ΔMTS
***
0
2.5
5
7.5
10
CJ No. / um of
Mito Circumference

e

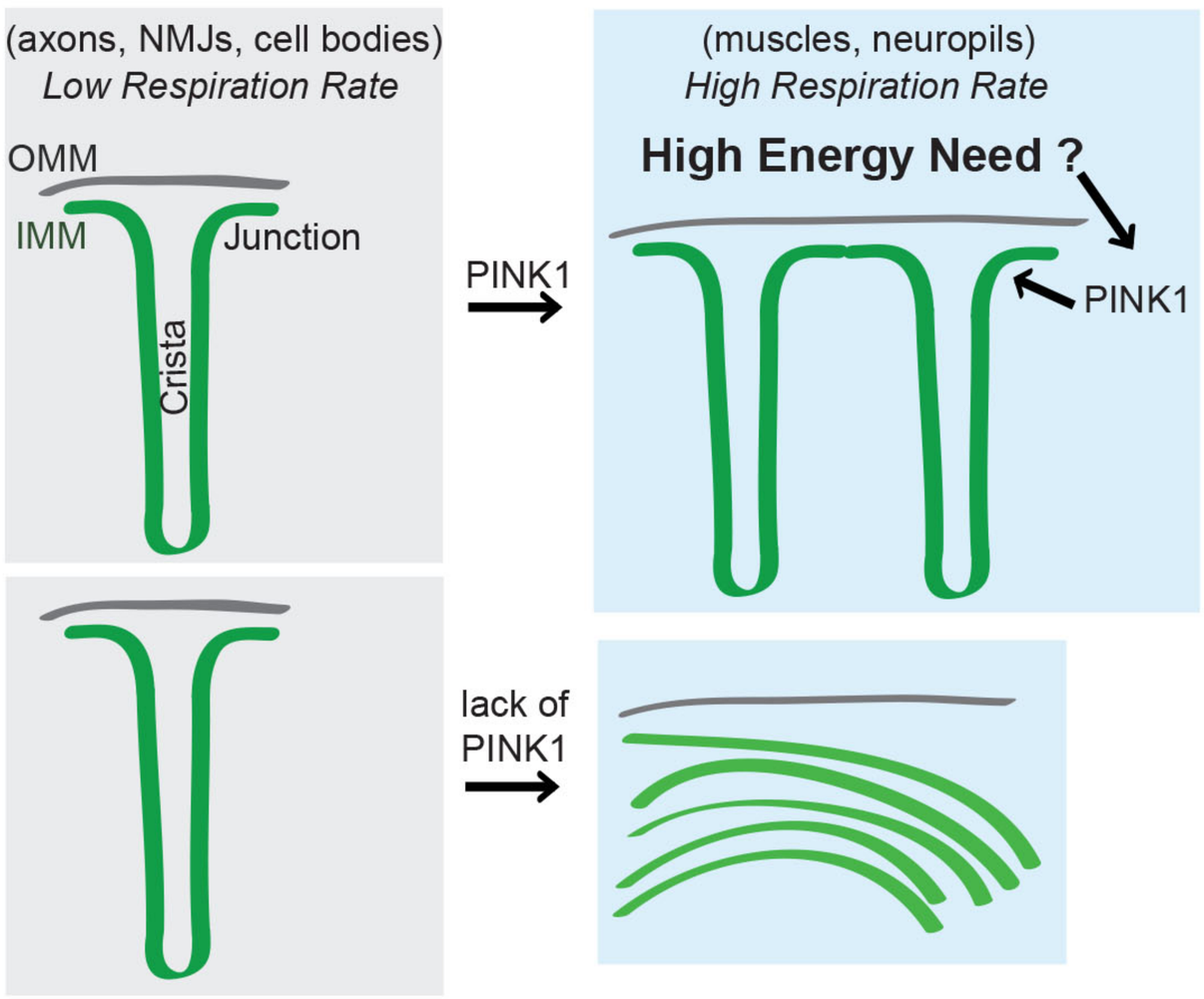
Late Third Instar Larvae
(axons, NMJs, cell bodies)
Low Respiration Rate
(muscles, neuropils)
High Respiration Rate
High Energy Need ?
OMM
IMM
Junction
Crista
PINK1
PINK1
lack of
PINK1

f

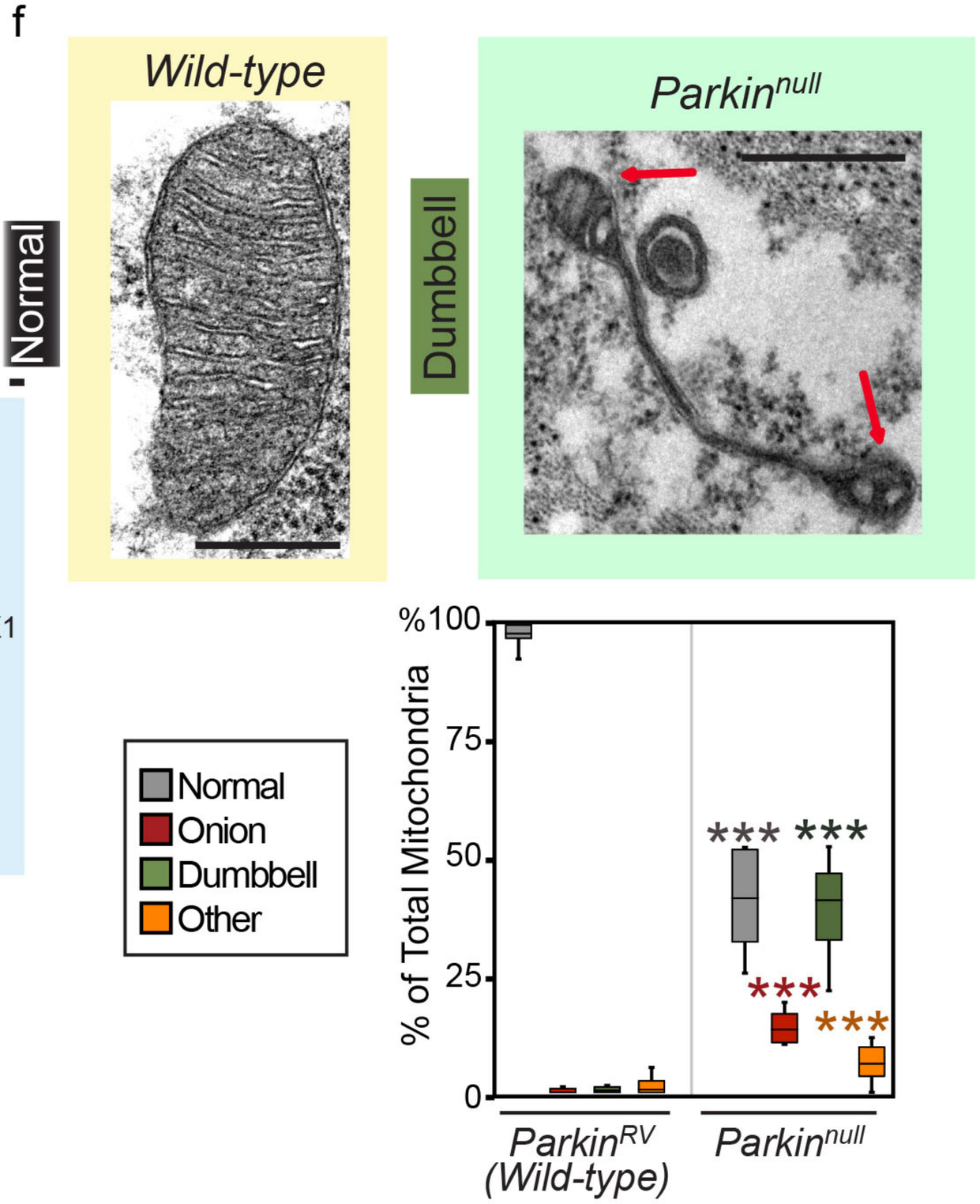
Wild-type
Parkinnull
Normal
Dumbbell
Normal
Onion
Dumbbell
Other
%100
75
50
25
0
% of Total Mitochondria
***
***
***
***
ParkinRV
(Wild-type)
Parkinnull

a

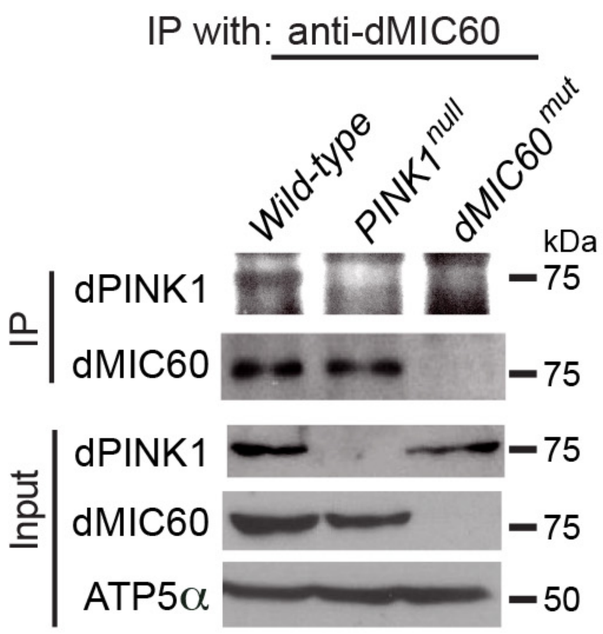
IP with: anti-dMIC60
Wild-type
PINK1null
dMIC60mut
kDa
IP
dPINK1
dMIC60
Input
dPINK1
dMIC60
ATP5α
75
75
75
75
50

b

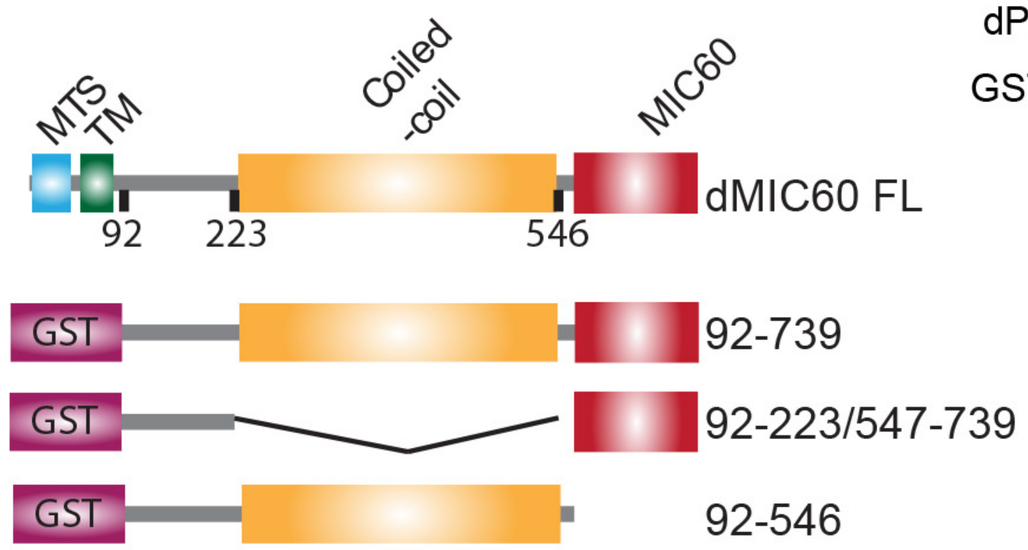
MTS
TM
Coiled
-coil
MIC60
dMIC60 FL
92
223
546
GST
92-739
GST
92-223/547-739
GST
92-546

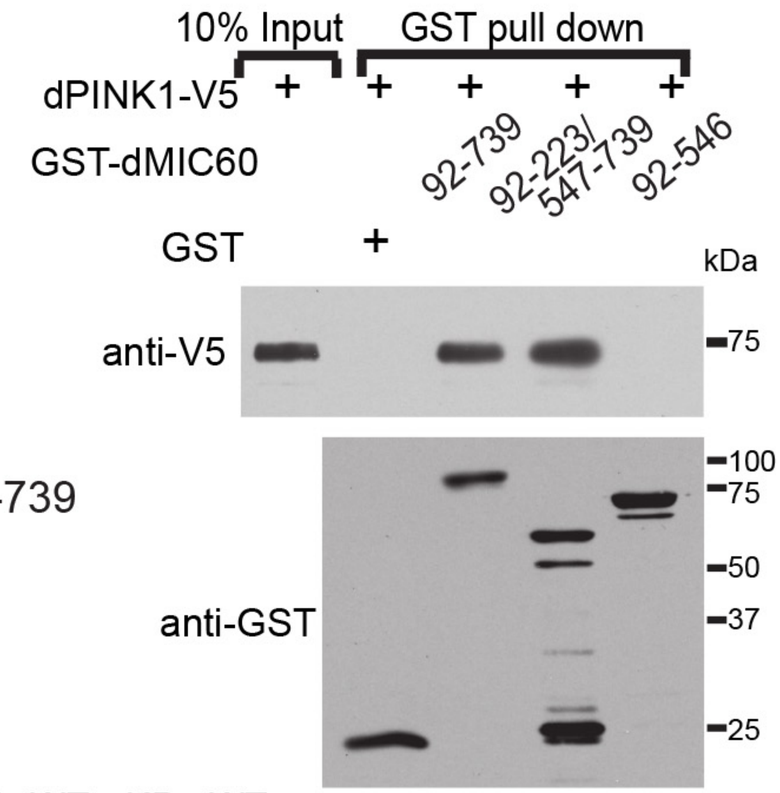
10% Input
GST pull down
dPINK1-V5
GST-dMIC60
92-739
92-223/
547-739
92-546
GST
kDa
anti-V5
anti-GST
75
100
75
50
37
25

c

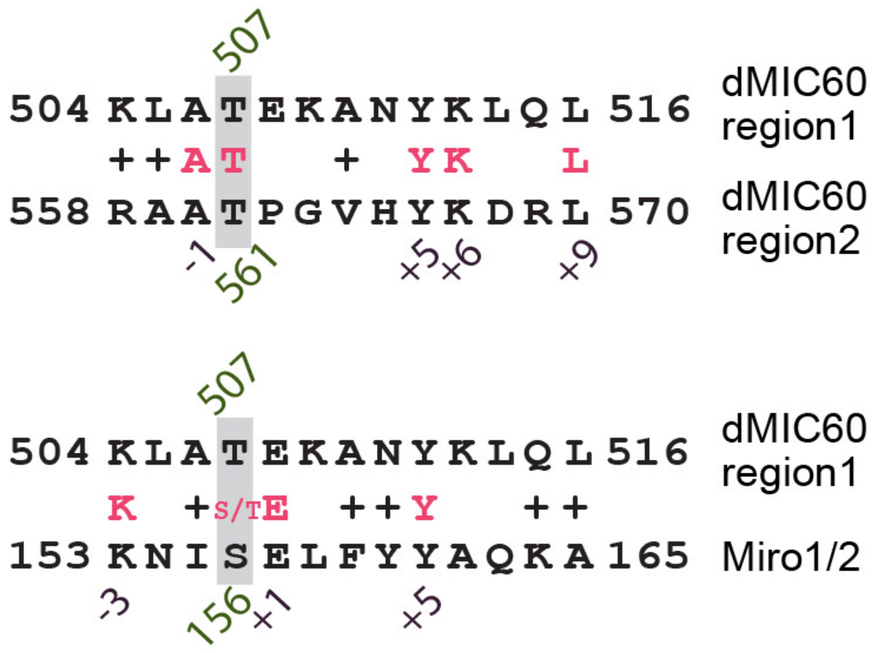
507
504 K L A T E K A N Y K L Q L 516
+ + A T + Y K L
558 R A A T P G V H Y K D R L 570
-1
561
+5
+6
+9
dMIC60
region1
dMIC60
region2
507
504 K L A T E K A N Y K L Q L 516
K +S/TE ++ Y ++
153 K N I S E L F Y Y A Q K A 165
-3
156
+1
+5
dMIC60
region1
Miro1/2

d

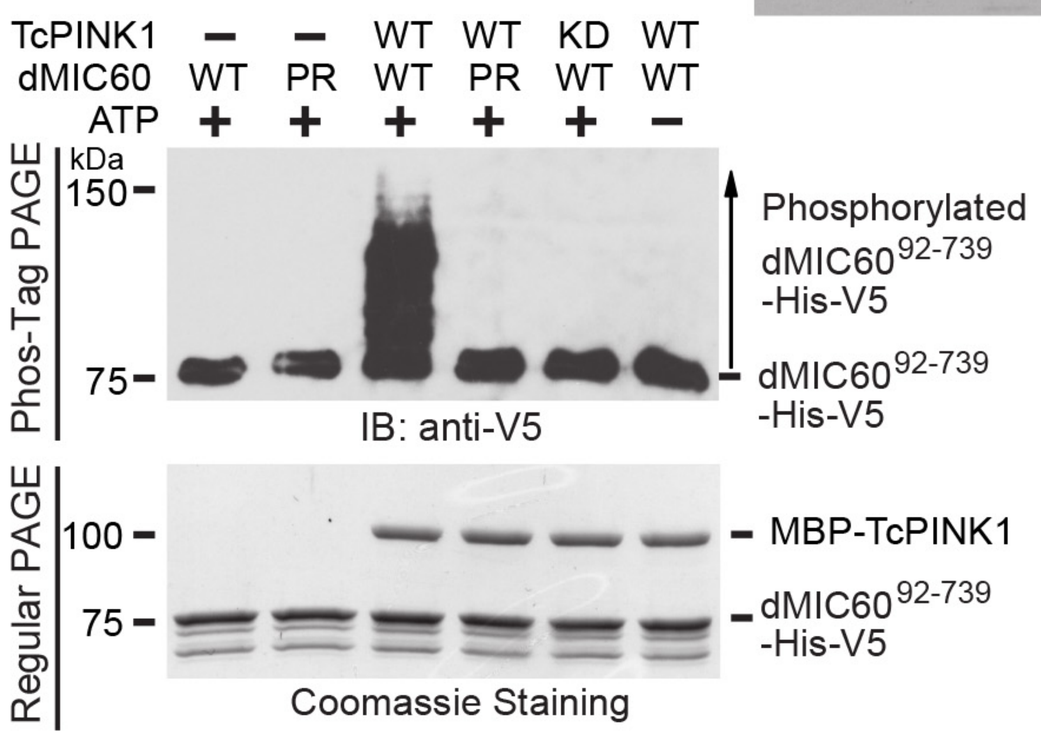
TcPINK1 – – WT WT KD WT
dMIC60 WT PR WT PR WT WT
ATP + + + + + –
kDa
150
75
Phos-Tag PAGE
Phosphorylated
dMIC60 92-739
-His-V5
dMIC60 92-739
-His-V5
IB: anti-V5
Regular PAGE
100
75
MBP-TcPINK1
dMIC60 92-739
-His-V5
Coomassie Staining

e

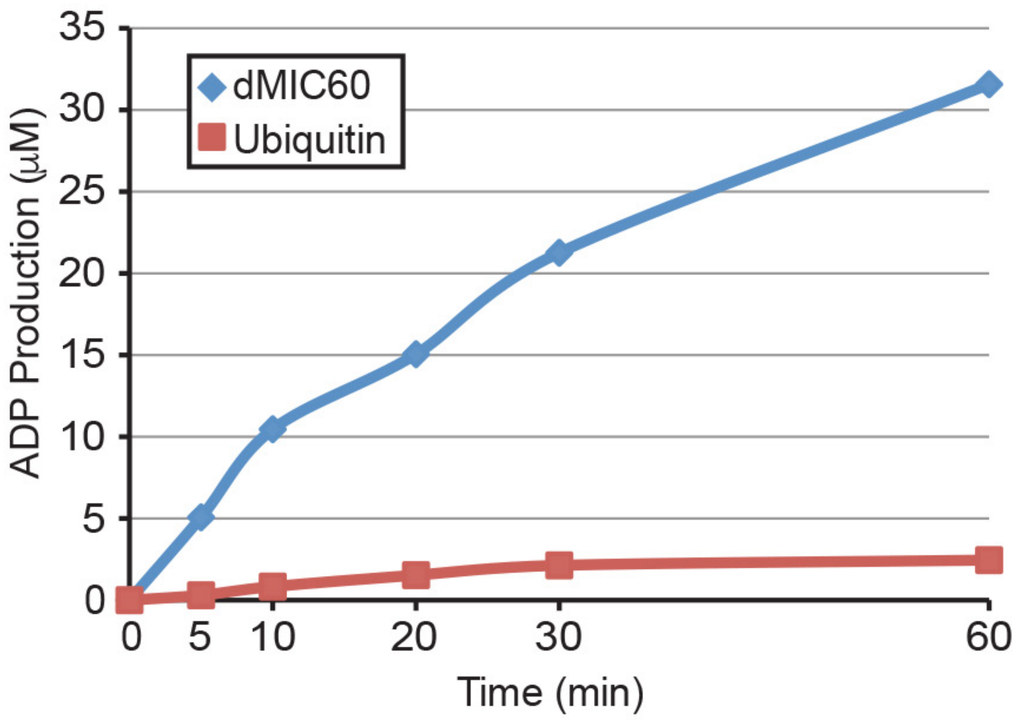
dMIC60
Ubiquitin
ADP Production (μM)
35
30
25
20
15
10
5
0
0
5
10
20
30
60
Time (min)

f

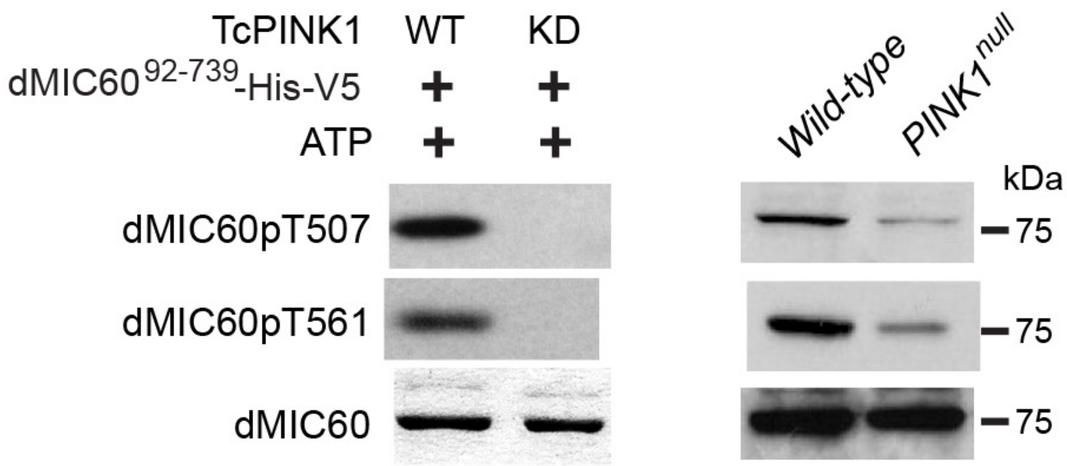
TcPINK1 WT KD
dMIC60 92-739 -His-V5 + +
ATP + +
dMIC60pT507
dMIC60pT561
dMIC60
Wild-type
PINK1null
kDa
75
75
75


Normalized dMIC60pT507 Level
Wild-type
PINK1null
**
0
0.25
0.5
0.75
1
Normalized dMIC60pT561 Level
**
0
0.25
0.5
0.75
1

g

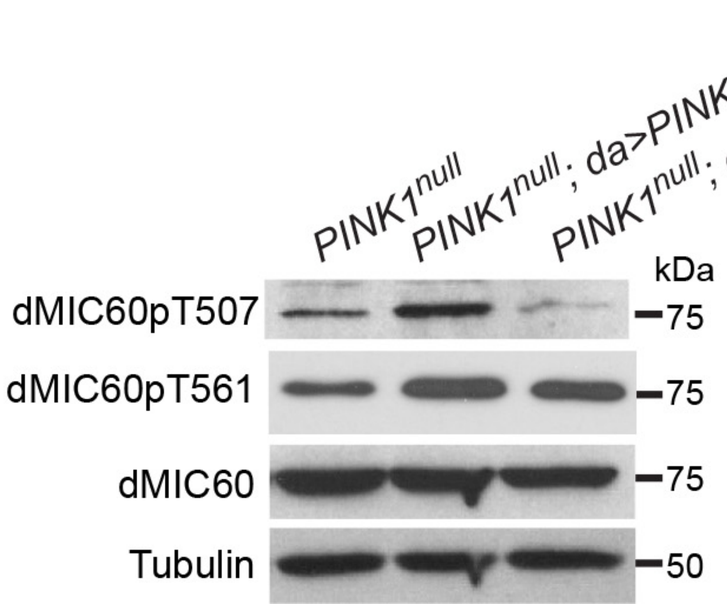
PINK1null
PINK1null; da>PINK1WT
PINK1null; da>PINK1ΔMTS
kDa
dMIC60pT507
dMIC60pT561
dMIC60
Tubulin
75
75
75
50

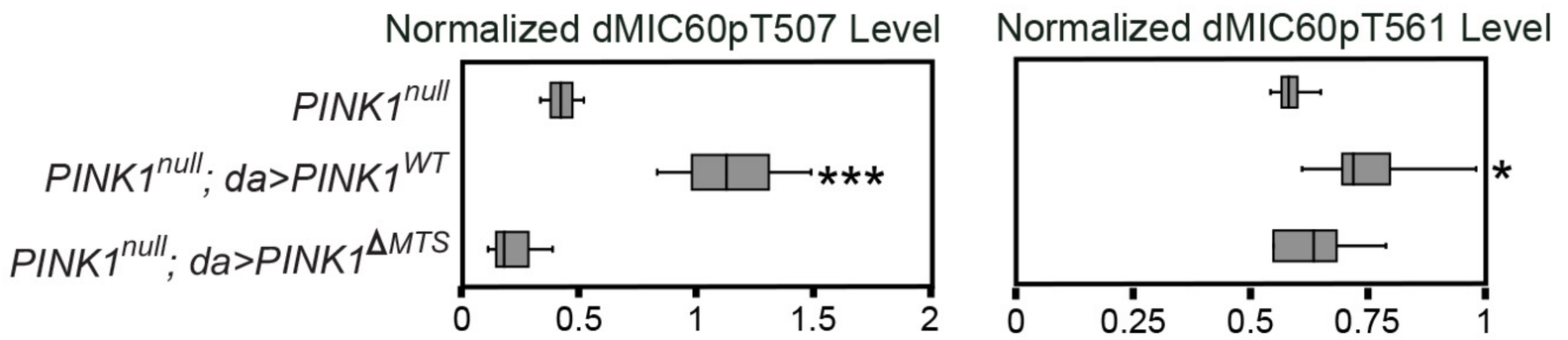
Normalized dMIC60pT507 Level
PINK1null
PINK1null; da>PINK1WT
PINK1null; da>PINK1ΔMTS
***
0
0.5
1
1.5
2
Normalized dMIC60pT561 Level
*
0
0.25
0.5
0.75
1

a

Muscles | VNC Neuropils | VNC Cell Bodies | NMJs | Segmental Nerves

dMIC60^{mut}

dMIC60^{mut}, *dMIC60*^{WT}

dMIC60^{mut}, *dMIC60*^{PR}

b

CJ No. / um of Mito Circumference

10
7.5
5
2.5
0

***
***

Muscles

c

% of Total Mitochondria That Are Onion

%
100
75
50
25
0

*** *** *** *** *** ***

Muscles | VNC Neuropils | VNC Cell Bodies | NMJs | Segmental Nerves

Wild-type | *dMIC60*^{mut} | *dMIC60*^{mut},*dMIC60*^{WT} | *dMIC60*^{mut},*dMIC60*^{PR}

a

PINK1^{null}/Y; da-GAL4

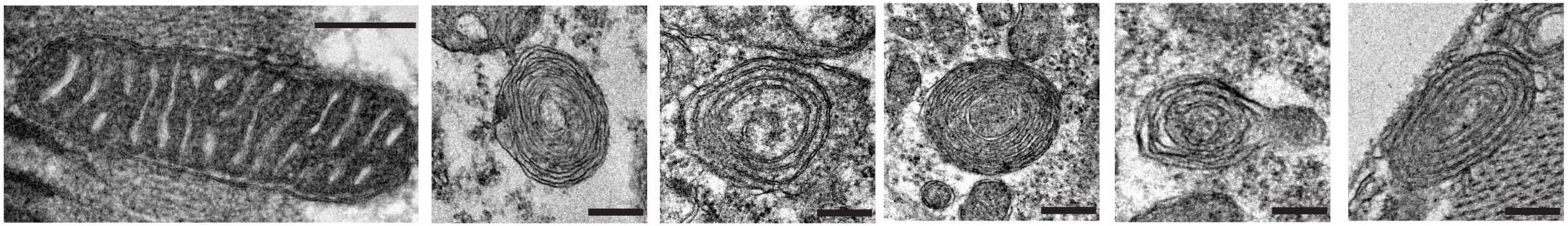

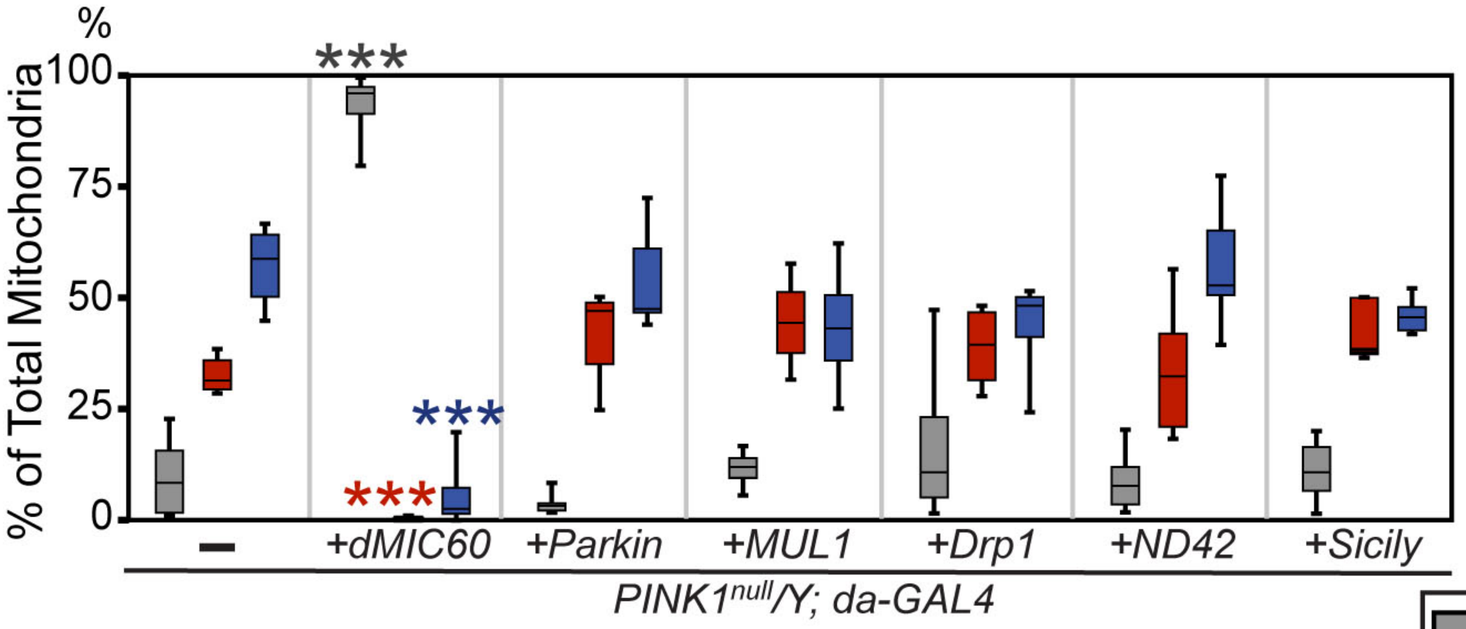

b

Tub>PINK1; dMIC60^{mut}

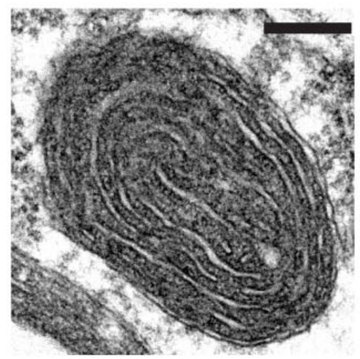

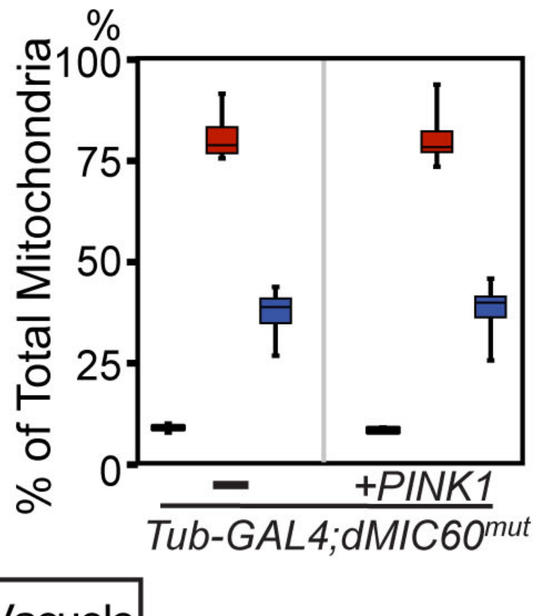

c

Parkin^{null}; da>dMIC60

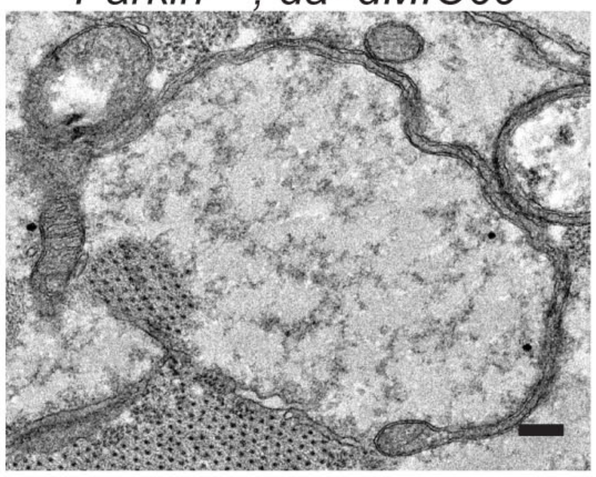

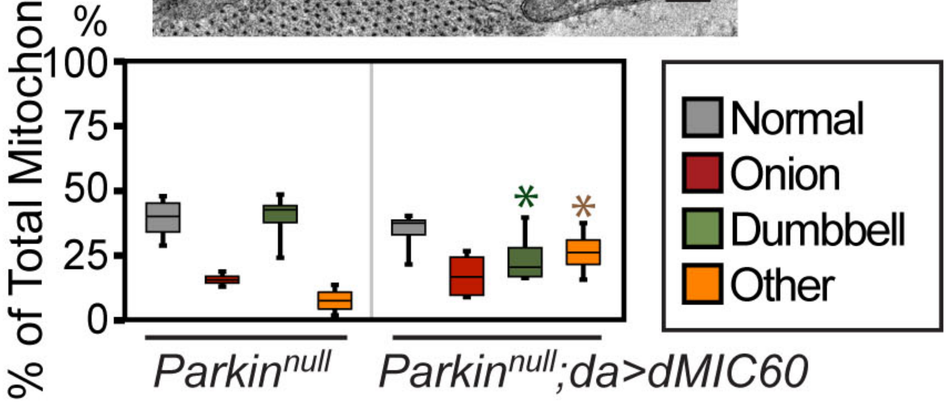

d

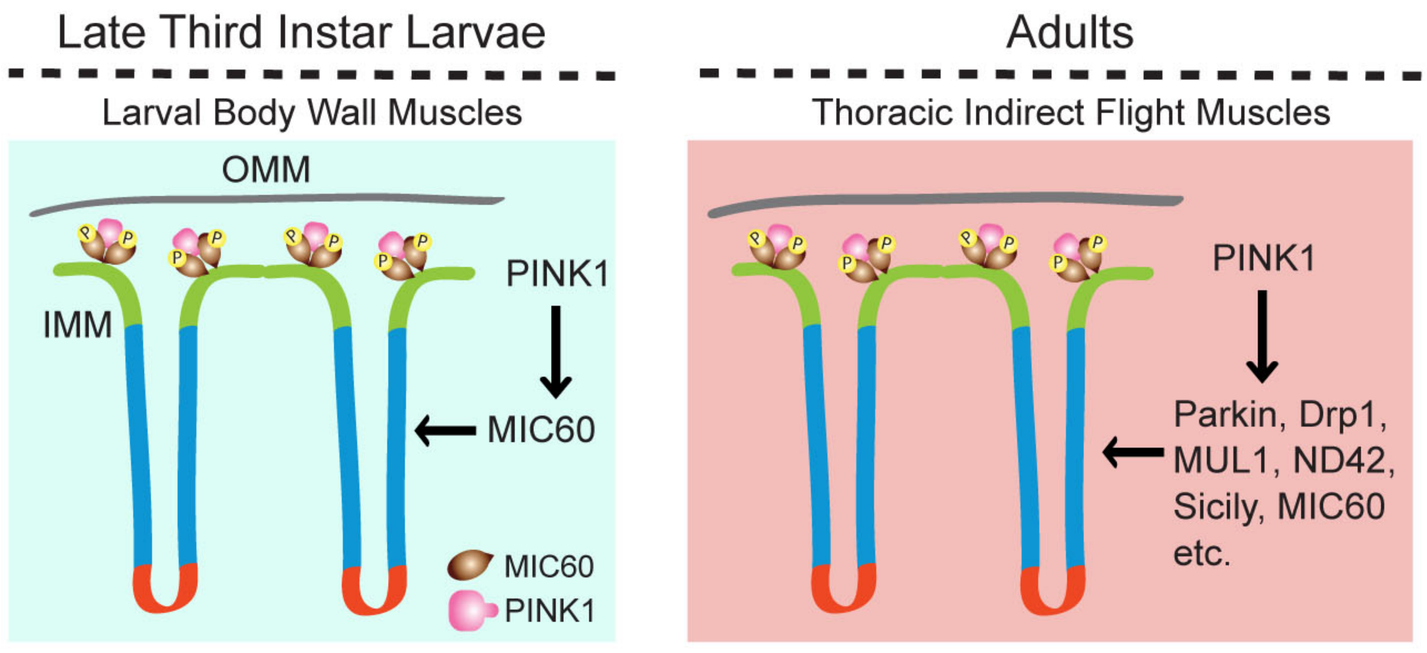

a

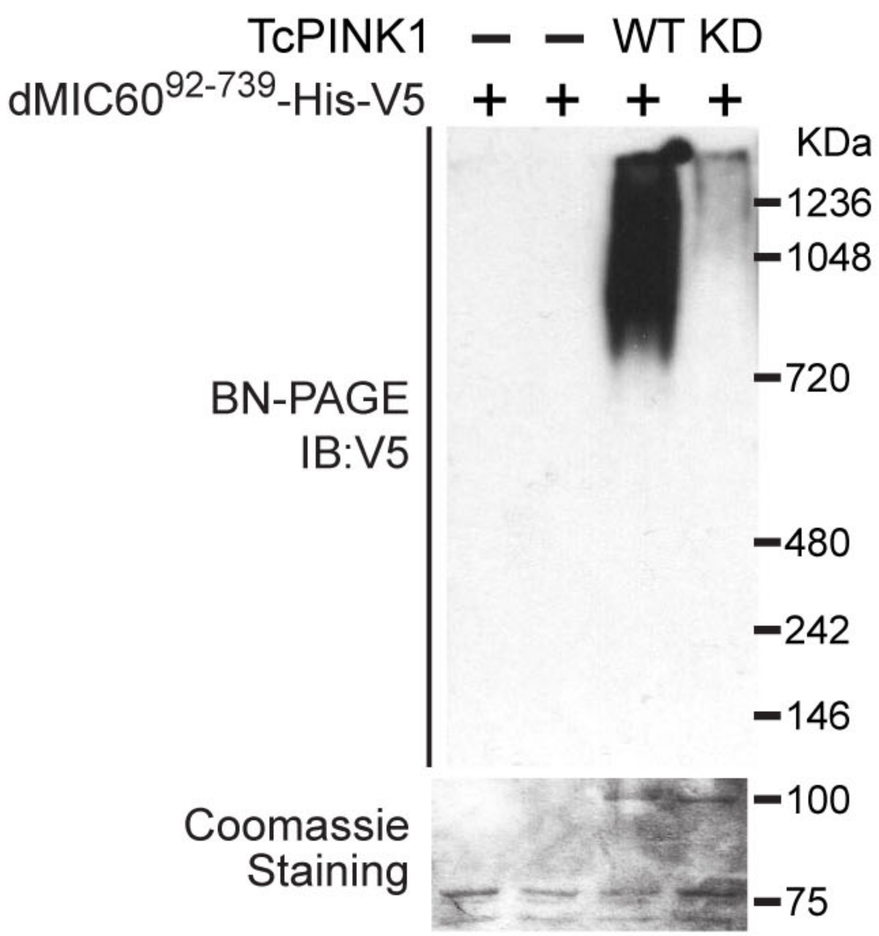
TcPINK1 – – WT KD
dMIC60^92-739-His-V5 + + + +
KDa
1236
1048
720
480
242
146
BN-PAGE
IB:V5
100
75
Coomassie
Staining

b

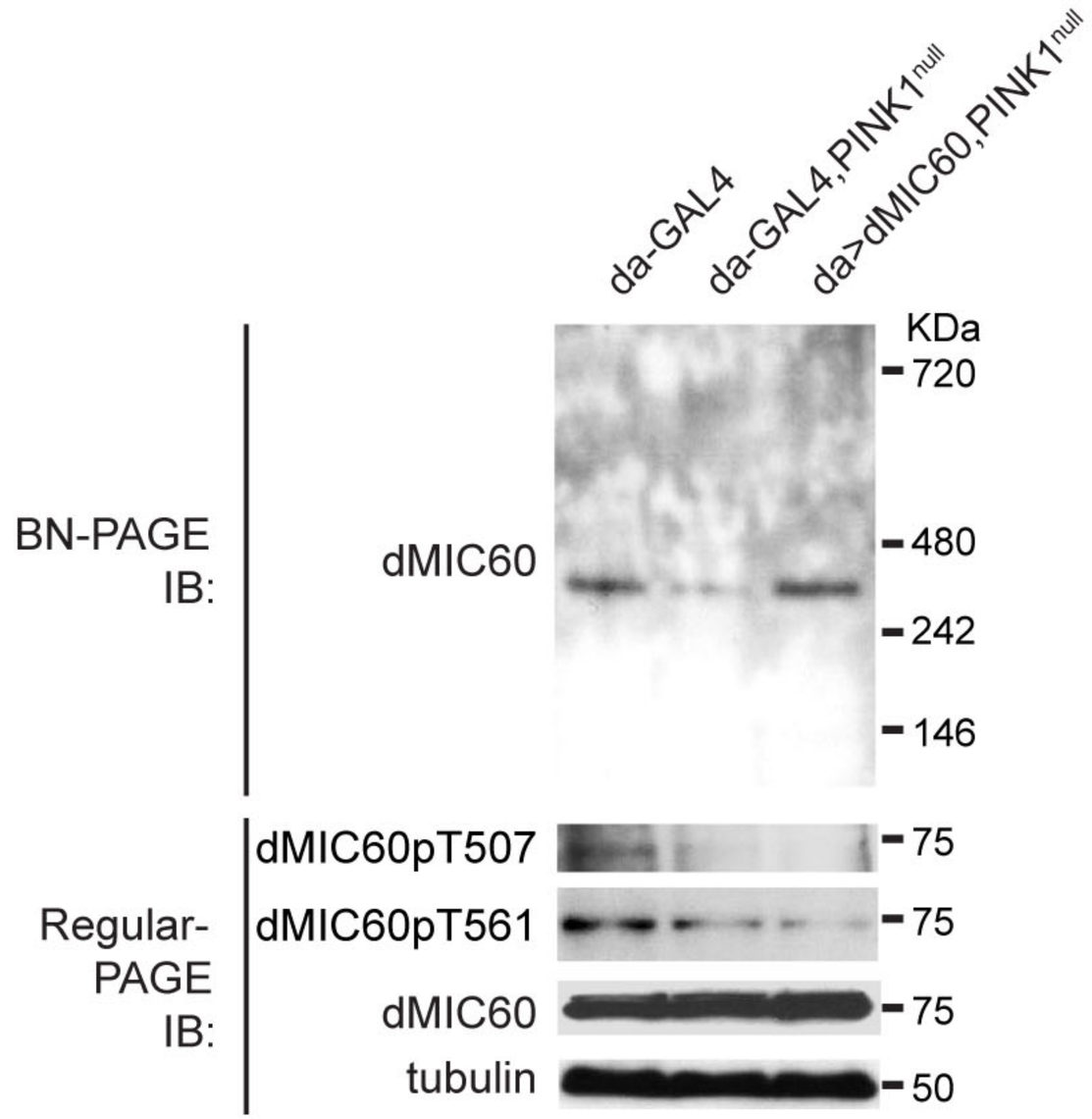
da-GAL4
da-GAL4,PINK1^null
da>dMIC60,PINK1^null
KDa
720
480
242
146
BN-PAGE
IB:
dMIC60
75
75
Regular-
PAGE
IB:
dMIC60pT507
dMIC60pT561
dMIC60
tubulin
75
50

c

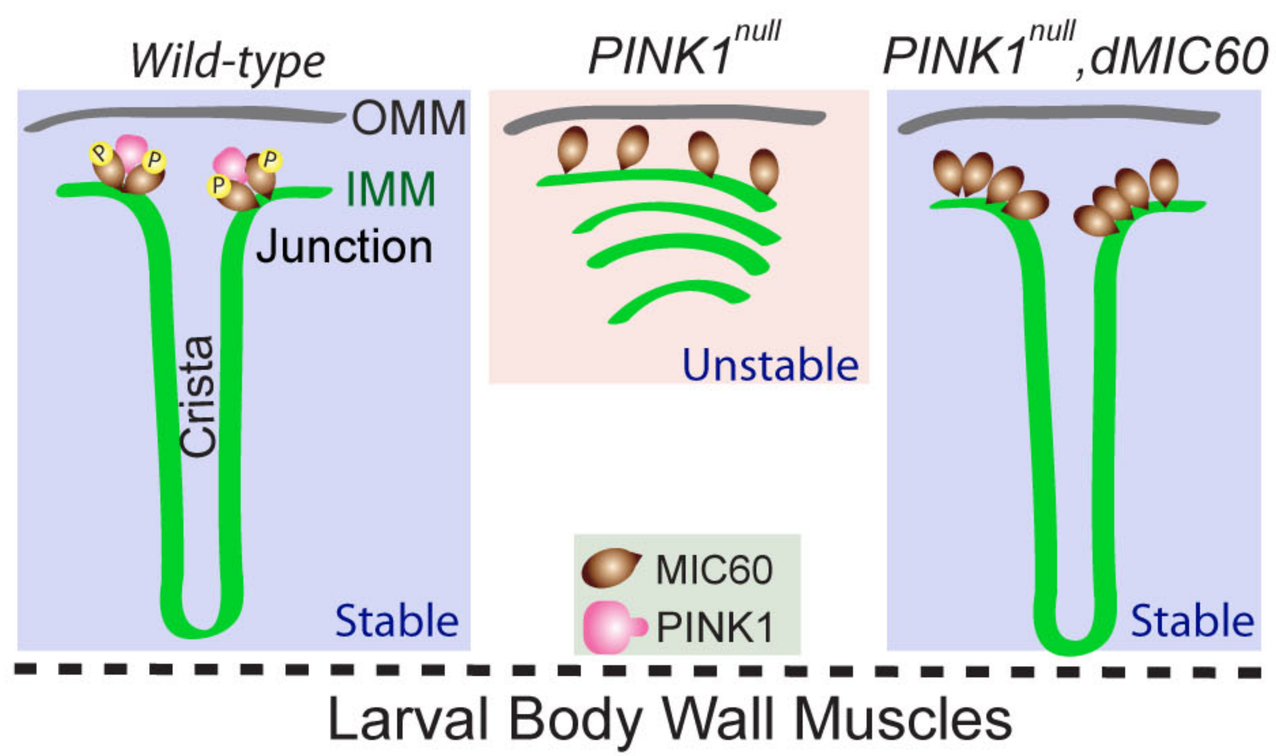
Wild-type
PINK1^null
PINK1^null,dMIC60
OMM
IMM
Junction
Crista
P
Stable
Unstable
MIC60
PINK1
Stable
Larval Body Wall Muscles

d

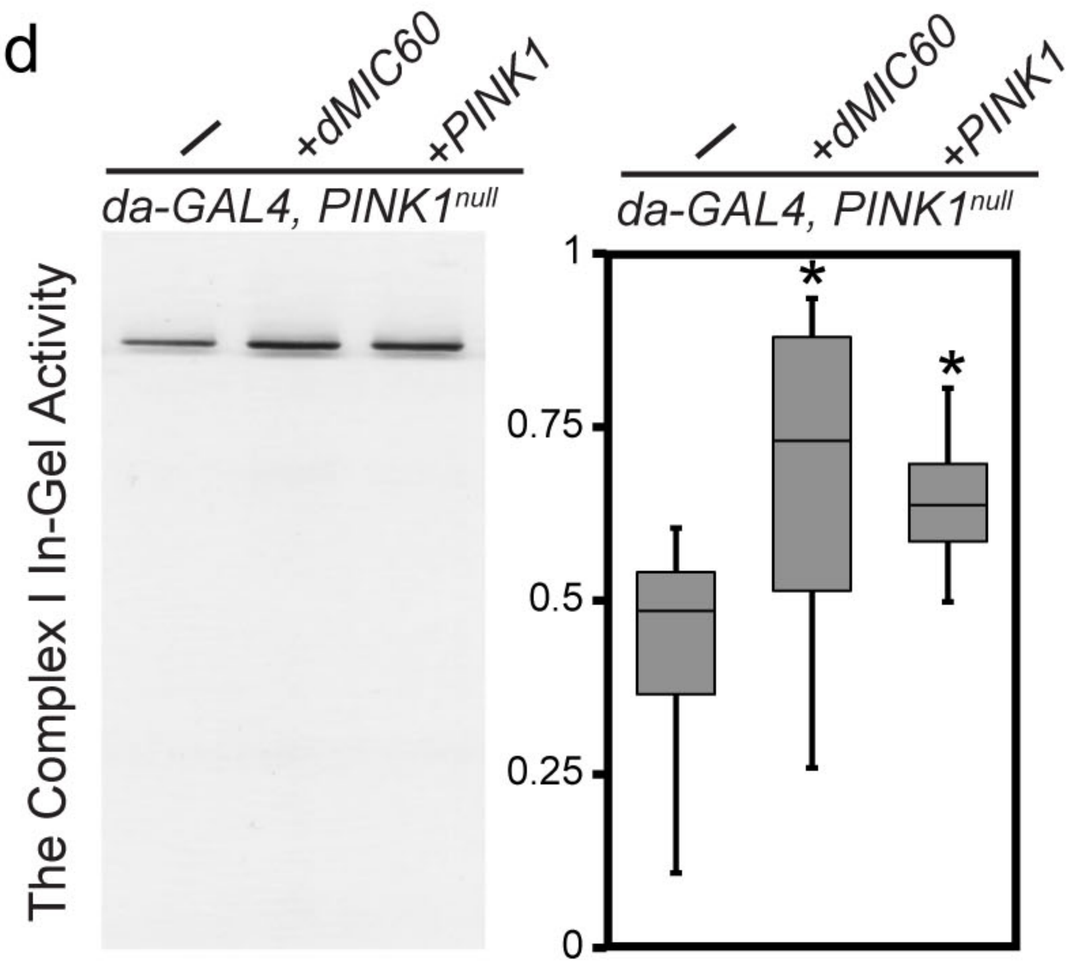
–
+dMIC60
+PINK1
da-GAL4, PINK1^null
The Complex I In-Gel Activity
1
0.75
0.5
0.25
0
*
*

a

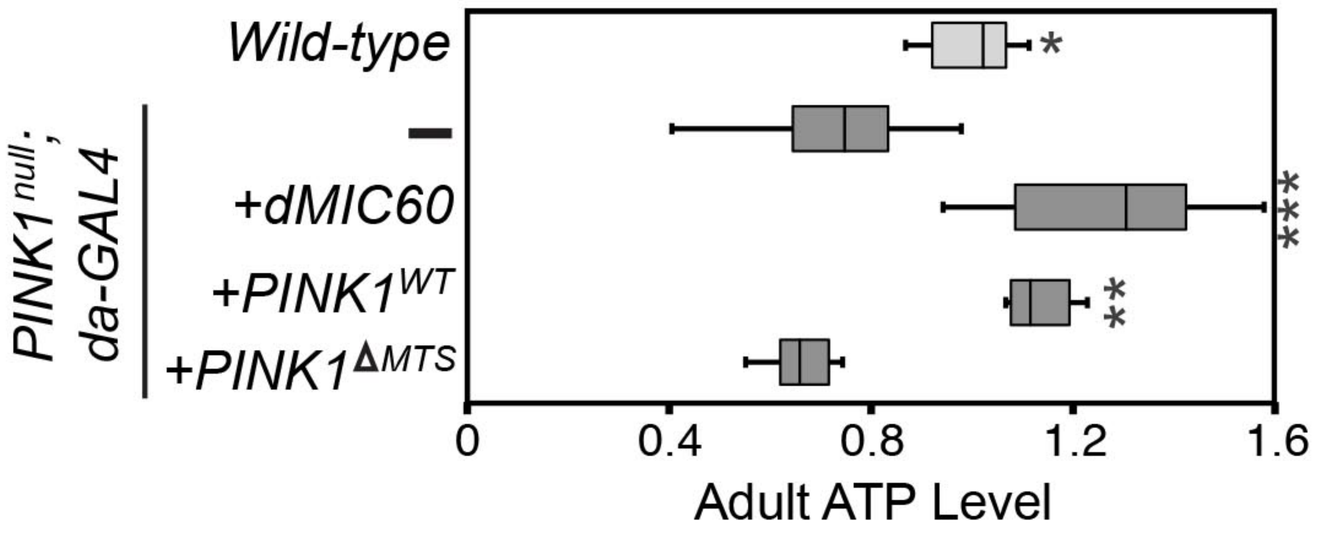
Wild-type
PINK1null; da-GAL4
–
+dMIC60
+PINK1WT
+PINK1ΔMTS
0
0.4
0.8
1.2
1.6
Adult ATP Level

b

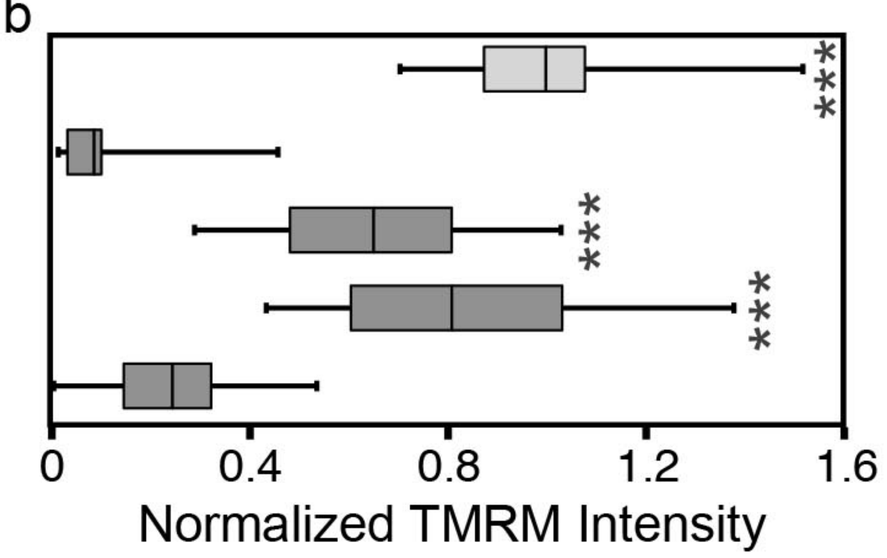
0
0.4
0.8
1.2
1.6
Normalized TMRM Intensity

c

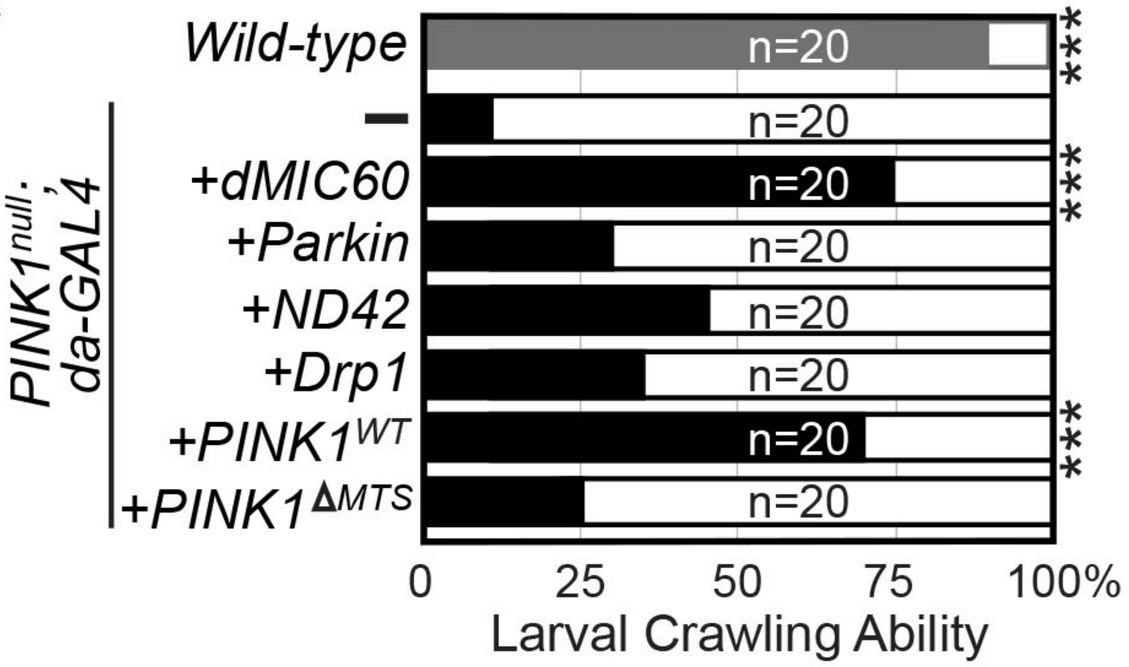
Wild-type
PINK1null; da-GAL4
–
+dMIC60
+Parkin
+ND42
+Drp1
+PINK1WT
+PINK1ΔMTS
n=20
0
25
50
75
100%
Larval Crawling Ability

d

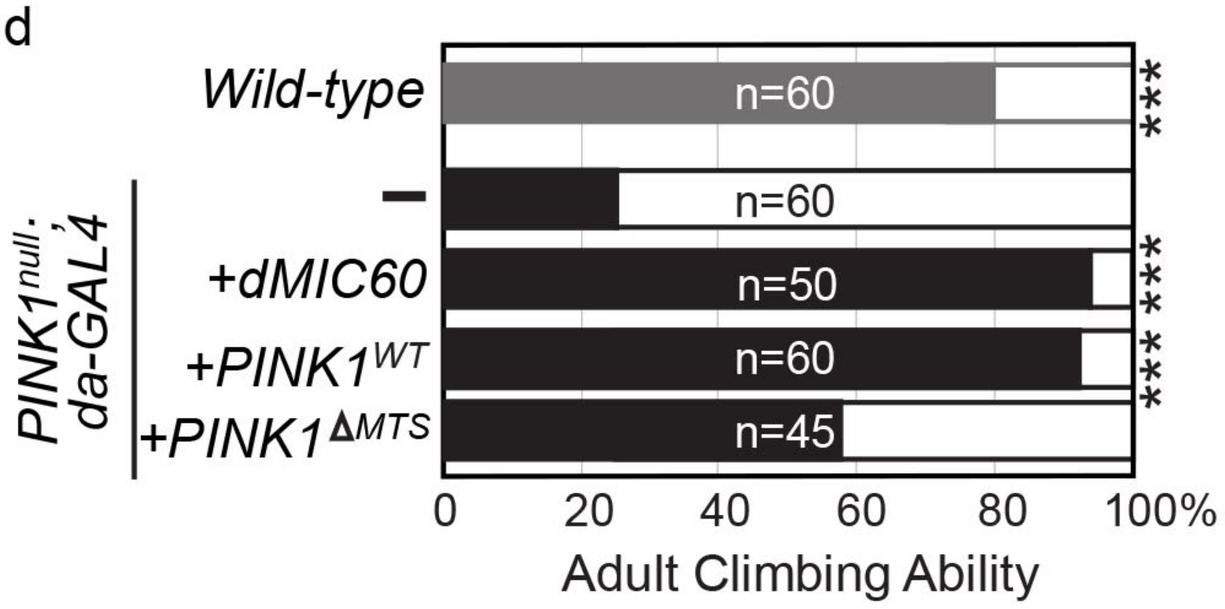
Wild-type
PINK1null; da-GAL4
–
+dMIC60
+PINK1WT
+PINK1ΔMTS
n=60
n=50
n=45
0
20
40
60
80
100%
Adult Climbing Ability

e

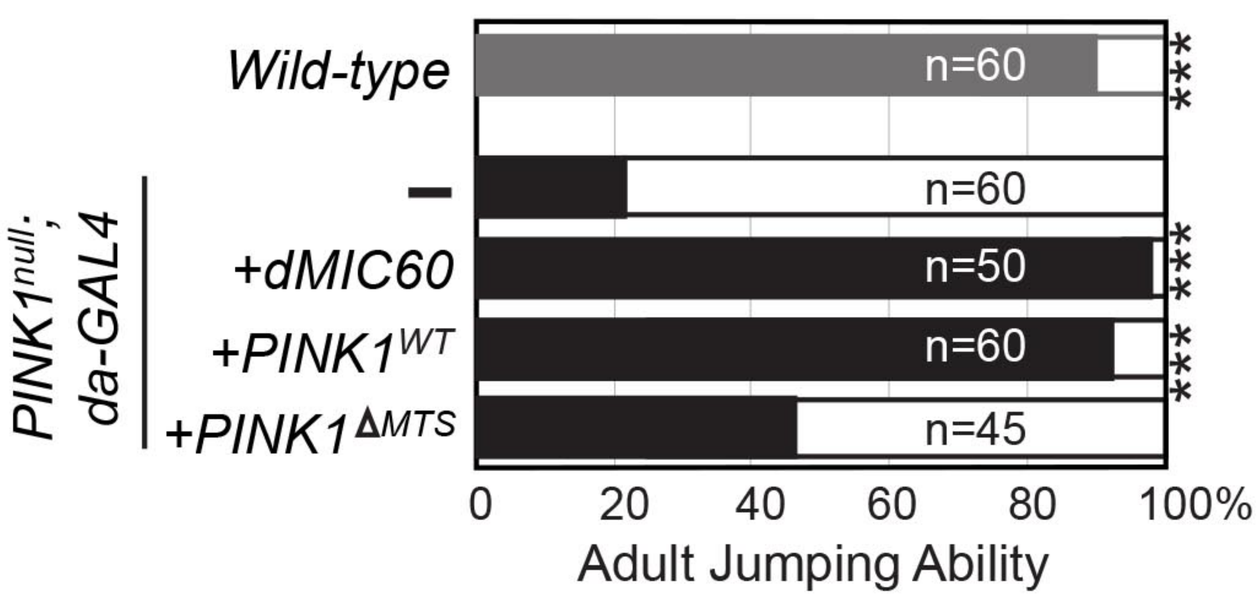
Wild-type
PINK1null; da-GAL4
–
+dMIC60
+PINK1WT
+PINK1ΔMTS
n=60
n=50
n=45
0
20
40
60
80
100%
Adult Jumping Ability

f

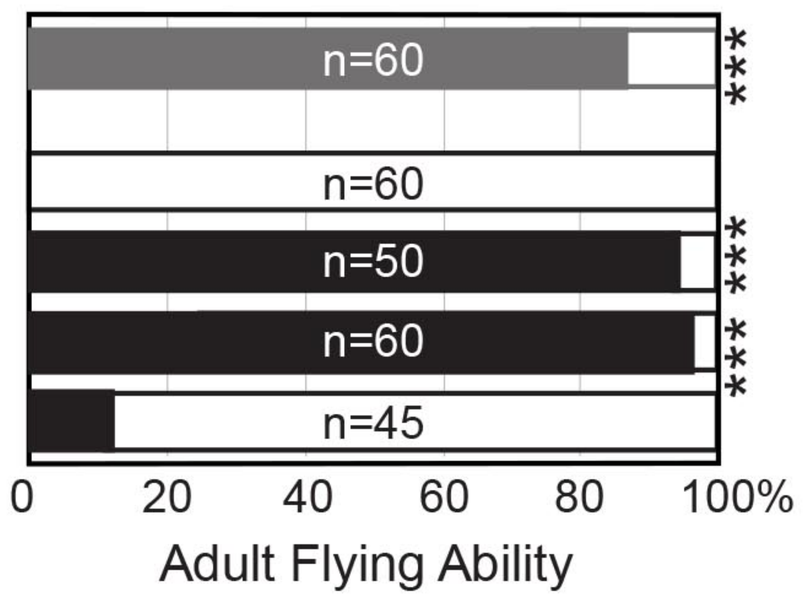
n=60
n=50
n=45
0
20
40
60
80
100%
Adult Flying Ability

g

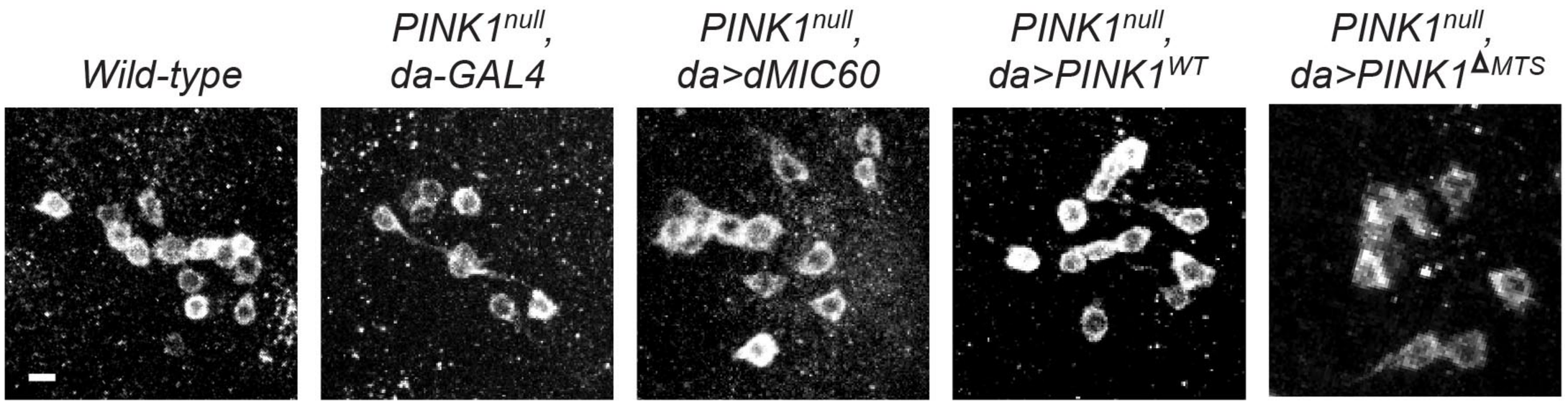
Wild-type
PINK1null, da-GAL4
PINK1null, da>dMIC60
PINK1null, da>PINK1WT
PINK1null, da>PINK1ΔMTS

h

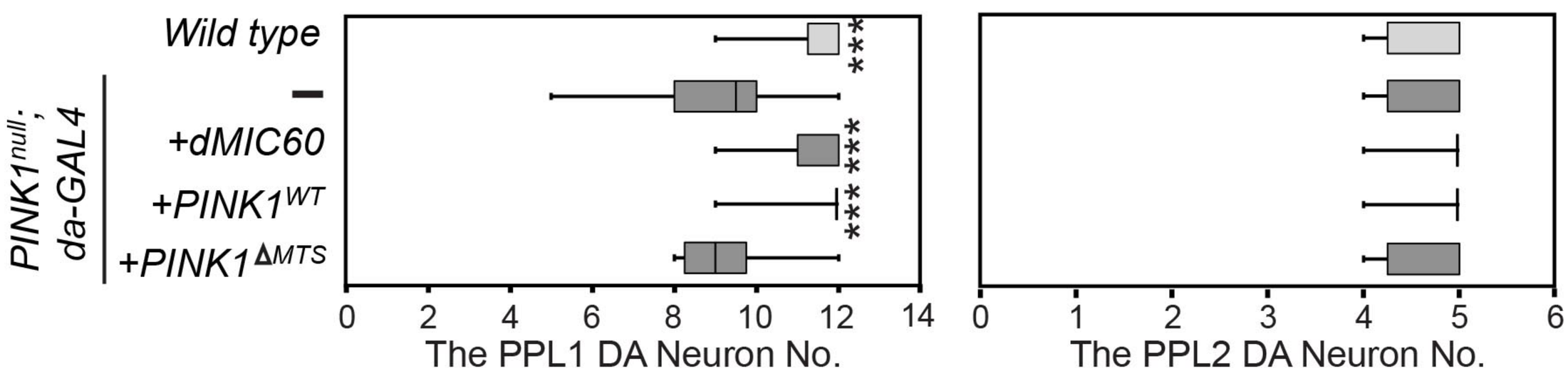
Wild type
PINK1null; da-GAL4
–
+dMIC60
+PINK1WT
+PINK1ΔMTS
0
2
4
6
8
10
12
14
The PPL1 DA Neuron No.
0
1
2
3
4
5
6
The PPL2 DA Neuron No.

a

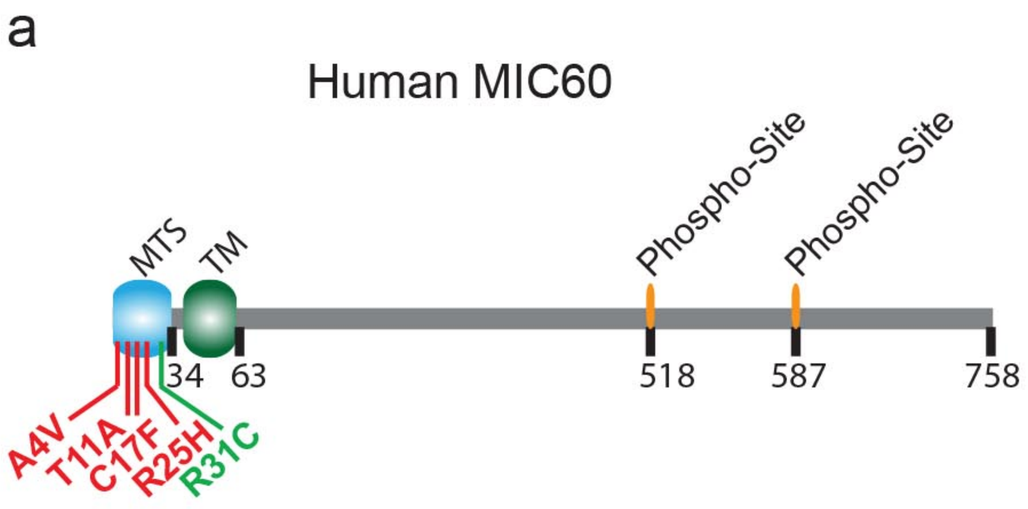
Human MIC60
MTS
TM
Phospho-Site
Phospho-Site
34
63
518
587
758
A4V
T11A
C17F
R25H
R31C

b

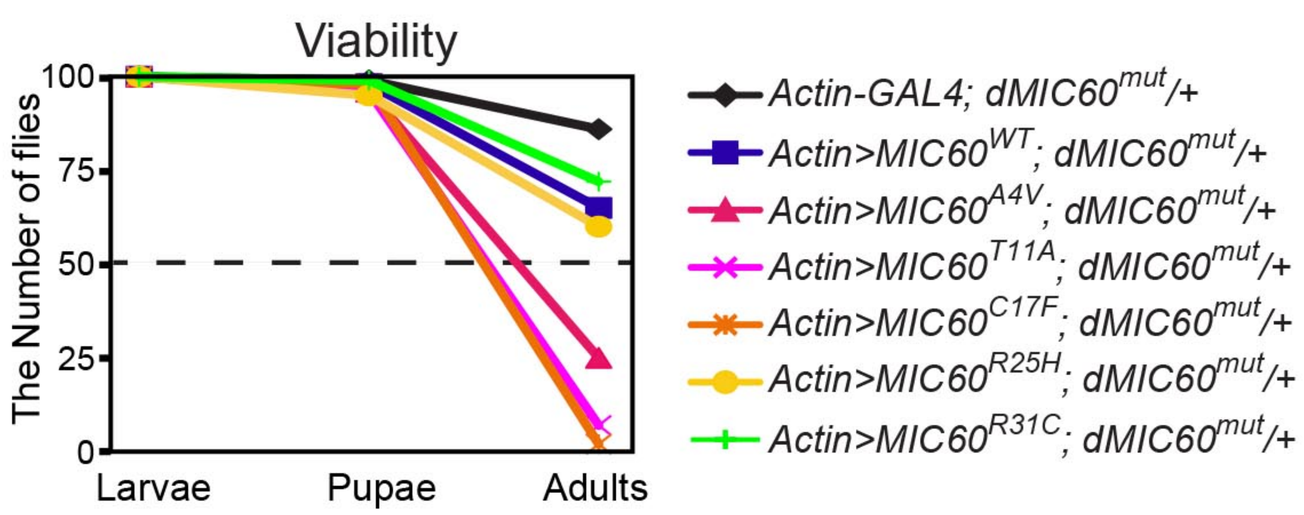
Viability
The Number of flies
100
75
50
25
0
Larvae
Pupae
Adults
Actin-GAL4; dMIC60mut/+
Actin>MIC60WT; dMIC60mut/+
Actin>MIC60A4V; dMIC60mut/+
Actin>MIC60T11A; dMIC60mut/+
Actin>MIC60C17F; dMIC60mut/+
Actin>MIC60R25H; dMIC60mut/+
Actin>MIC60R31C; dMIC60mut/+

c

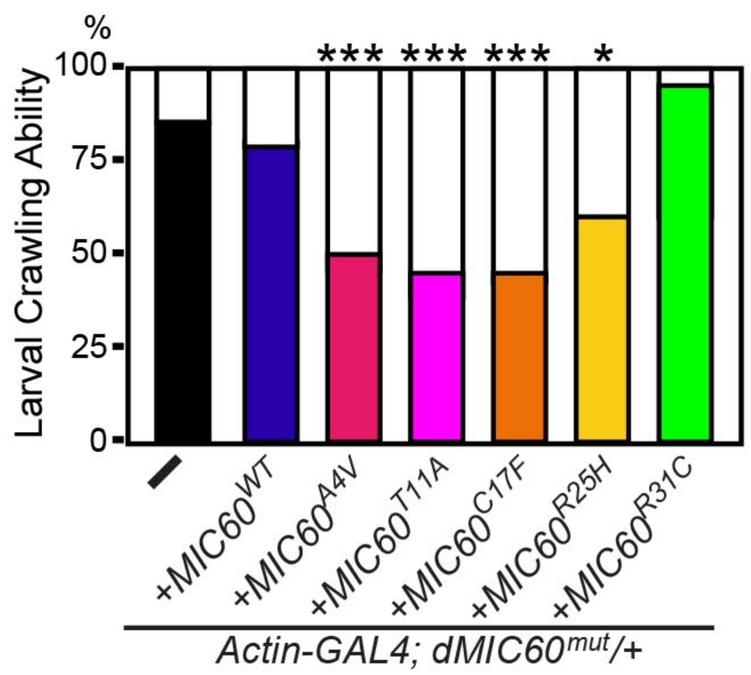
Larval Crawling Ability
%
100
75
50
25
0
*** *** *** *
+MIC60WT
+MIC60A4V
+MIC60T11A
+MIC60C17F
+MIC60R25H
+MIC60R31C
Actin-GAL4; dMIC60mut/+

d

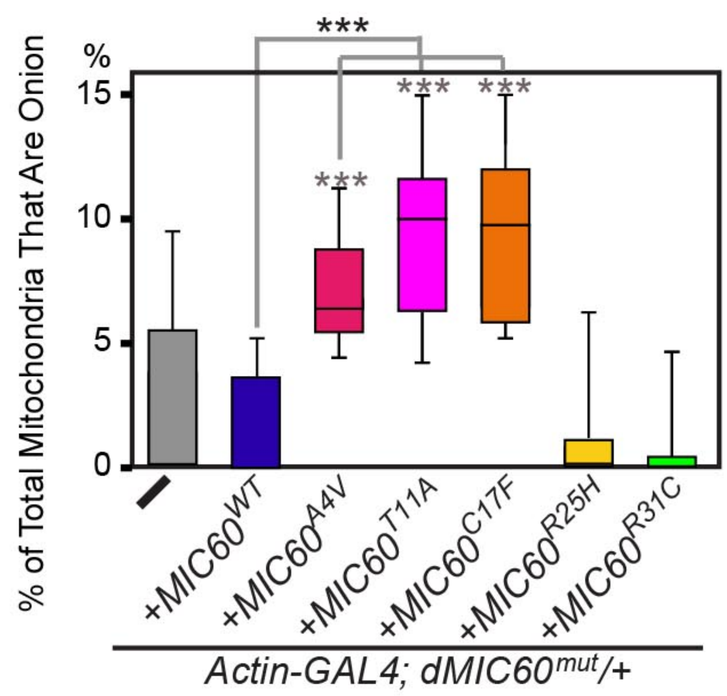
% of Total Mitochondria That Are Onion
%
15
10
5
0
***
*** ***
***
+MIC60WT
+MIC60A4V
+MIC60T11A
+MIC60C17F
+MIC60R25H
+MIC60R31C
Actin-GAL4; dMIC60mut/+

e

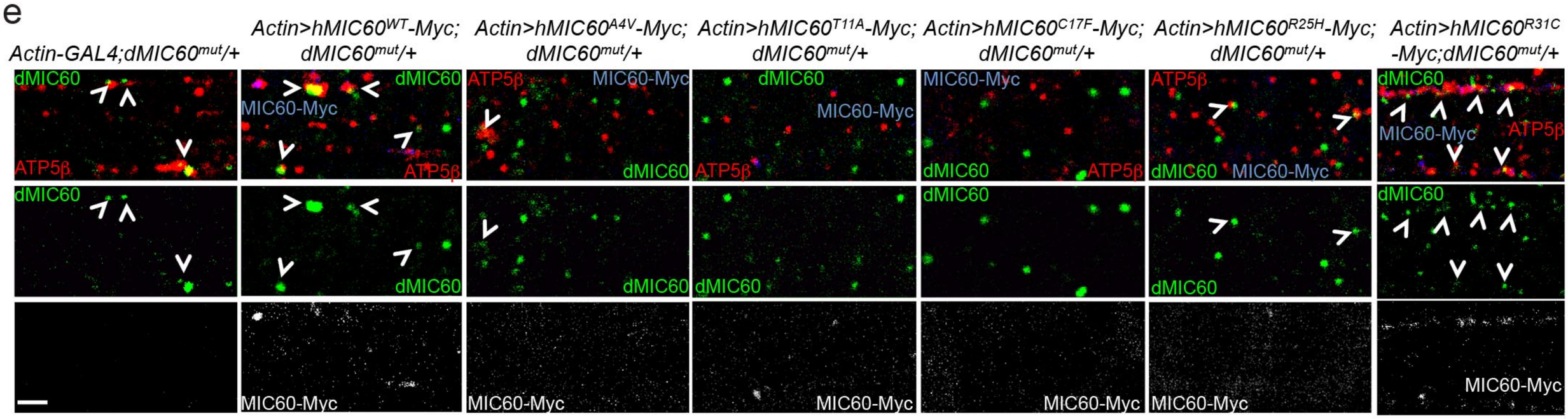
Actin-GAL4;dMIC60mut/+
Actin>hMIC60WT-Myc; dMIC60mut/+
Actin>hMIC60A4V-Myc; dMIC60mut/+
Actin>hMIC60T11A-Myc; dMIC60mut/+
Actin>hMIC60C17F-Myc; dMIC60mut/+
Actin>hMIC60R25H-Myc; dMIC60mut/+
Actin>hMIC60R31C -Myc;dMIC60mut/+
dMIC60
ATP5β
MIC60-Myc

f

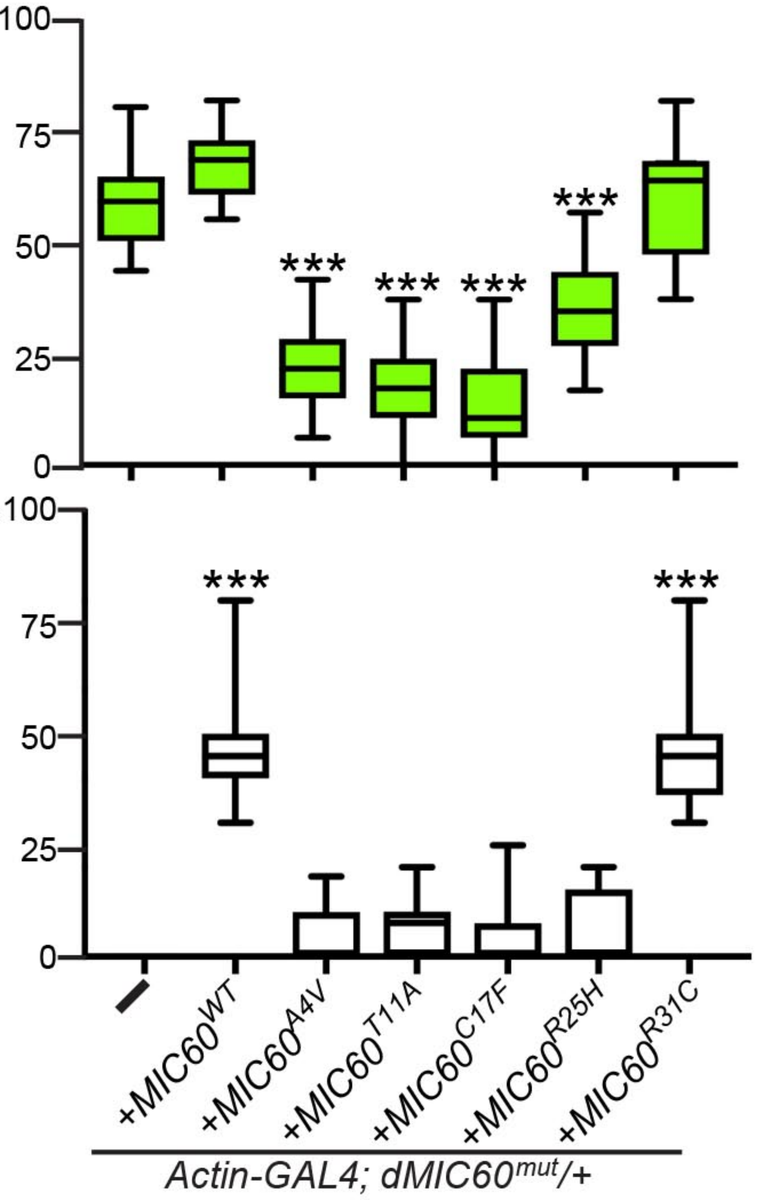
% of ATP5β Puncta Positive for dMIC60
% of ATP5β Puncta Positive for MIC60-Myc
%100
75
50
25
0
*** *** *** *** ***
+MIC60WT
+MIC60A4V
+MIC60T11A
+MIC60C17F
+MIC60R25H
+MIC60R31C
Actin-GAL4; dMIC60mut/+

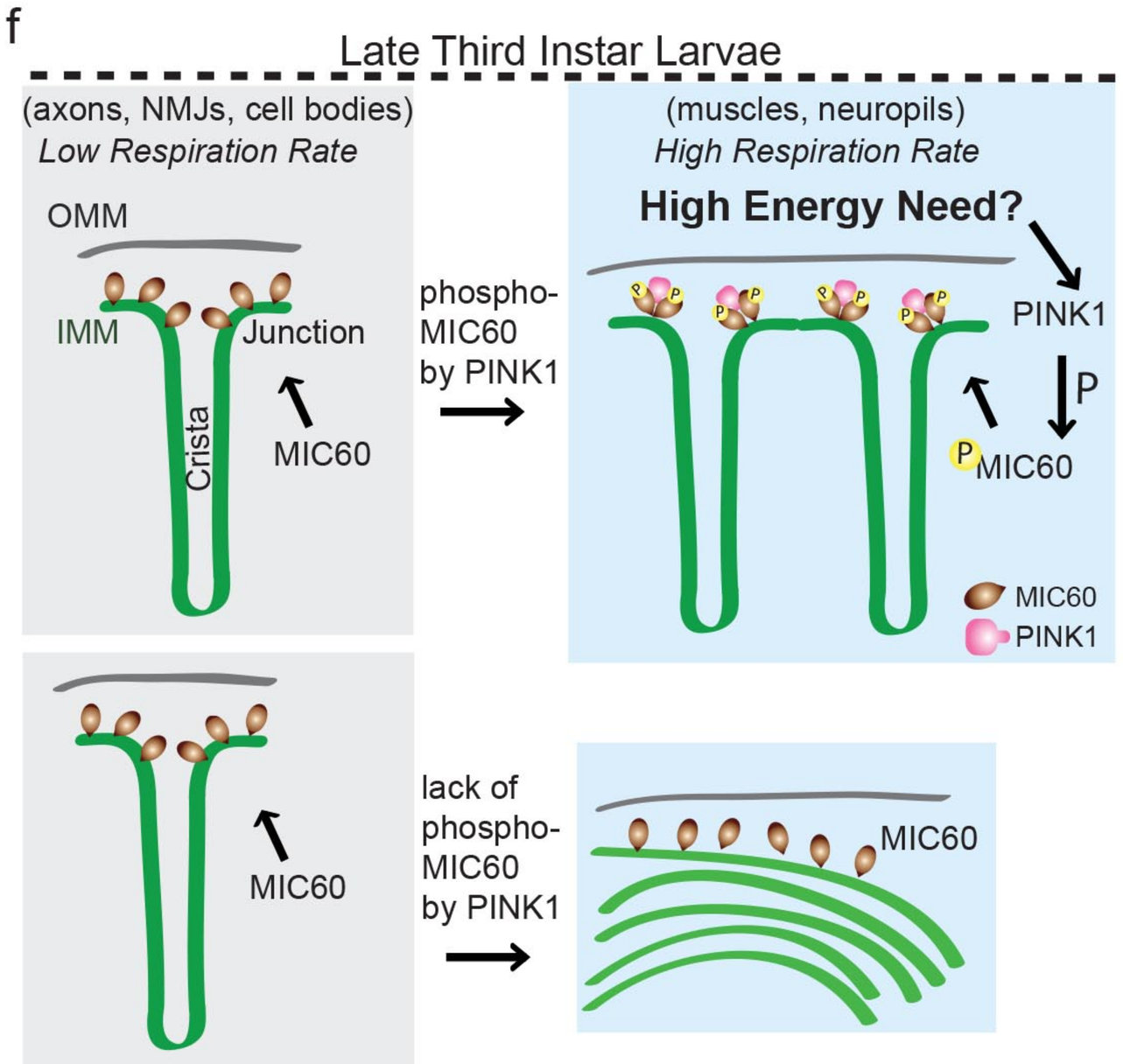
Late Third Instar Larvae
(axons, NMJs, cell bodies)
Low Respiration Rate
OMM
IMM
Junction
Crista
MIC60
phospho-MIC60 by PINK1
(muscles, neuropils)
High Respiration Rate
High Energy Need?
PINK1
P
MIC60
MIC60
PINK1
MIC60
lack of phospho-MIC60 by PINK1
MIC60